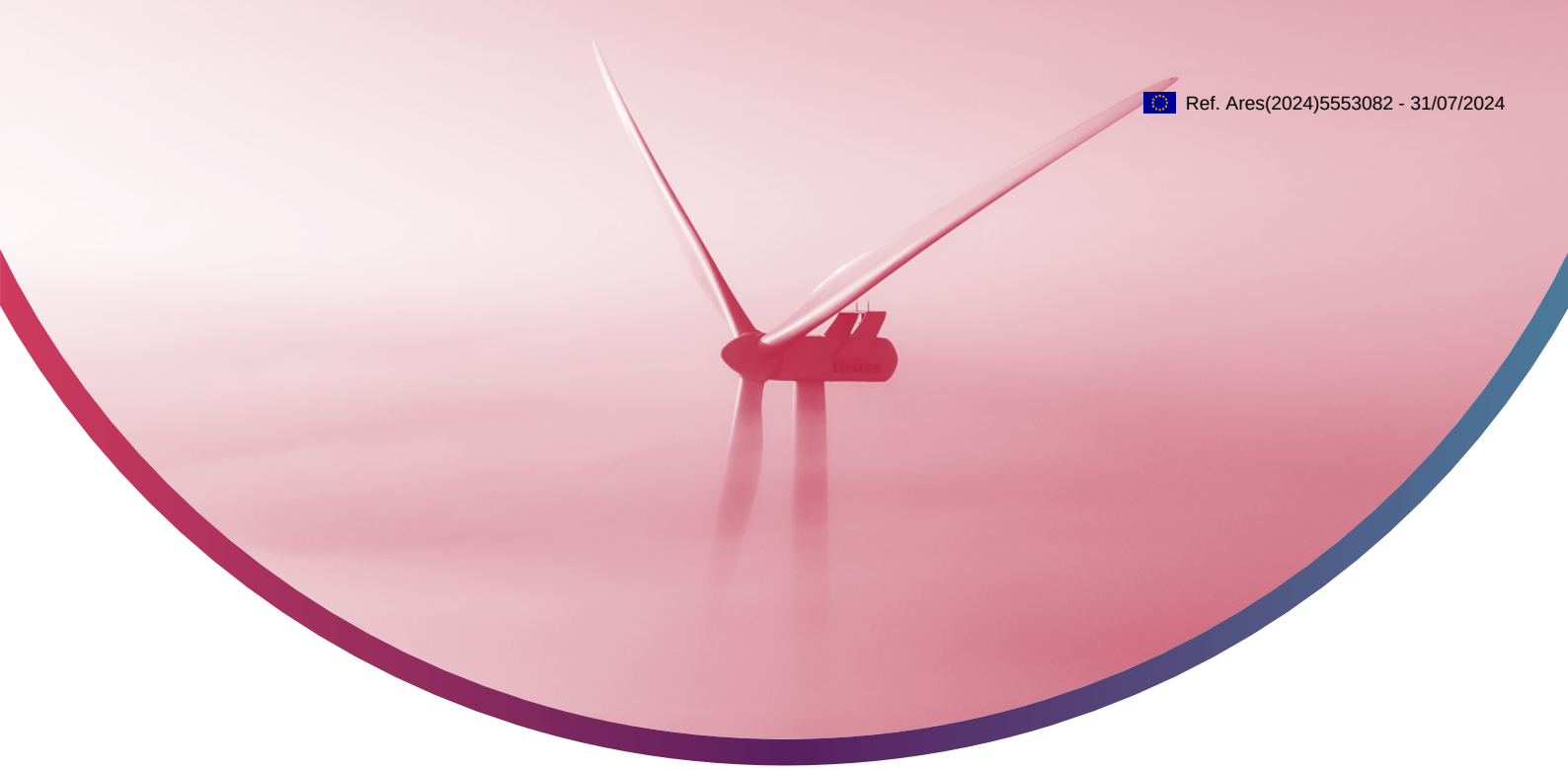

AiRE

D3.3 – Airfoil performance model operating with degraded surface caused by precipitation and calima

Development and improvement of models for blade aerodynamics operating with surface degradation

CENER | CENTRO NACIONAL DE ENERGÍAS RENOVABLES

DOCUMENT INFORMATION

PROJECT INFORMATION	
GRANT AGREEMENT NUMBER	101083716
PROJECT TITLE	Advanced study of the atmospheric flow Integrating REal climate conditions to enhance wind farm and wind turbine power production and increase components durability
PROJECT ACRONYM	AIRE
FUNDING SCHEME	HORIZON-RIA
PROJECT COORDINATOR	CENER
START DATE OF THE PROJECT	1 January 2023
DURATION	48 months
CALL IDENTIFIER	HORIZON-CL5-2021-D3-03
PROJECT WEBSITE	https://aire-project.eu/

DELIVERABLE INFORMATION	
DELIVERABLE N° & TITLE	D3.3 – Airfoil performance model operating with degraded surface caused by precipitation and calima
WP NO. & TITLE	WP3 – Development and extension of numerical models
WP LEADER	VTT
DELIVERABLE CREATOR	CENER
CONTRIBUTING PARTNERS	CENER, OREC, IWES, DUT, SGRE, PLOCAN
AUTHORS	Guillén Campaña, David Bretos and Ion Lizarraga
CONTRIBUTORS	CENER, OREC, IWES, DUT, SGRE, PLOCAN
REVIEWERS	CENER
CONTRACTUAL DEADLINE	31 July 2024
DELIVERY DATE TO EC	31 July 2024
DISSEMINATION LEVEL	Public

DOCUMENT LOG			
VERSION	DATE	AUTHOR	DESCRIPTION OF CHANGE
V0.1	9-Jul-2024	CENER (Guillen Campaña, David Bretos and Ion Lizarraga)	Initial version
V0.2	12-Jul-2024	CENER (Beatriz Méndez)	Review feedback
V1.1	16-Jul-2024	CENER (Guillen Campaña)	First version
V1.2	25-Jul_2024	OREC, IWES, DUT, SGRE, PLOCAN	Review feedback
V2.1	30-Jul-2024	CENER (Guillen Campaña, Beatriz Méndez)	Second version
V2.2	31-Jul-2024	INV (Laia Mencia, Estefanía González)	Review feedback
V3.1	31-Jul-2024	CENER (Beatriz Méndez)	Final version approval

DISCLAIMER

Funded by the European Union

"Funded by the European Union. Views and opinions expressed are however those of the author(s) only and do not necessarily reflect those of the European Union. Neither the European Union nor the granting authority can be held responsible for them."

CONTENT

Figure Index

Table index

Acronym Glossary

CFD: Computational Fluid Dynamics	**LER**: Leading-Edge Roughness
AEP: Annual Energy Production	**O&M**: Operation and Maintenance
APM: Airfoil Performance Model	**HPC**: High Performance Computing
ML: Machine Learning	**RF**: Random Forest
AoA: Angle of Attack	**NN**: Neural Network
LEP: Leading-Edge protection	**RMSE**: Root Mean Square Error
RET: Rain Erosion Test	**R2**: R-squared
LEE: Leading-Edge Erosion	

Consortium partners

	Partner	Country	Short name
1	Centro Nacional de Energías Renovables	Spain	CENER
2	Danmarks Tekniske Universitet	Denmark	DTU
3	Teknologian Tutkimuskeskus	Finland	VTT
4	Frauhofer Gesellschaft zur Forderung der Angewandten Forschung	Germany	IWES
5	Siemens Gamesa Renewable Energy	Denmark	OREC
6	Green Capital Power	Spain	CAPITAL
7	ENGIE	France	ENGIE
8	Consorcio para el diseño, construcción, equipamiento y explotación de la plataforma oceánica de Canarias	Spain	PLOCAN
9	Universidad de Las Palmas de Gran Canaria	Spain	ULPGC
10	Cartago Ventures	Spain	INV
11	Offshore Renewable Energy Catapult	UK	OREC

1 Introduction

Airfoil performance is very influenced by blade surface status. Flow is affected by the existence of roughness (due to dust or particles in the ambient) or by more severe blade damages (created by operation under wind and precipitation combined, especially in offshore sites). Firstly, a database will be created (CFD-airfoil) with the principal type of airfoil affections by climate, this will be done defining a representative roughness size of the elements placed on the blades or a typology characterization when a loss of blade material appears due to operation in real atmospheric conditions, this information will be obtained from blade inspections in the sites (WP2: dust in PLOCAN over the blades and blade status in the commercial farms). Secondly, a simplified airfoil performance model will be created that uses information from the data base so that the clean airfoil performance curves could be modified accounting for different surface and climate conditions. This simplified model will be the base to create the AEP and loads estimation tool under the specification of AIRE´s industrial partners.

The present deliverable is organised as follows. The first section, namely, evaluation of roughness effect in transitional flow, assess the aerodynamic performance of thin and thick airfoils and how to properly model this effect. The second section, blade loss of material during service life, consists of an analysis of blades in operation to determine how degraded the blades are and how to model the eroded surface of the airfoil. Finally, with the knowledge obtained from the previous two sections a simplified airfoil performance model is developed in order to estimate precisely the influence of the blade status on the aerodynamic performance.

The final objective of the task is the development of a simplified model of the effect of the blade distributed roughness or mass loss on the aerodynamic performance of an airfoil. The model is called Airfoil Performance Model (APM). The APM estimates the aerodynamic performance by means of machine learning (ML) algorithms taking into account the surface status of an airfoil. The aerodynamic coefficients considered are the lift and drag coefficients and the efficiency, defined as the ratio between lift and drag.

Three blade status are considered:

- Clean airfoil: no surface degradation is considered.
- Rough airfoil: uniformly distributed roughness over a certain part of the airfoil surface.
- Eroded airfoil: there exists a loss of material over a certain part of the airfoil surface.

As stated, the APM tool will be based on ML algorithms. The usual approach of a ML problem is:

1. Gathering data, i.e., the aerodynamic coefficients under a range of surface conditions.
2. Data preprocessing, which is intended to gain knowledge on the data.
3. Building datasets into training, validation and test sets.
4. Model development which requires to select the appropriate algorithm, train and refine the model using training and validation datasets.
5. Evaluation of the obtained model.

Some questions need to be answered prior to all those steps, they are collected in Table 1. There are two aspects that require of previous studies. Both erosion and roughness produce a degradation of the aerodynamic performance of an airfoil, nevertheless each status require a different modelling approach. Therefore, section 2 will analyse how the roughness affects to the aerodynamic performance while section 3.3 will cover the erosion analysis.

Table 1 Aspects to be considered before the APM development

Question	Answer
What is the objective of the tool?	The estimation of aerodynamic performance considering surface status. APM is intended to be able to estimate airfoils not considered within the database.
What kind of airfoils are going to be estimated?	Thin and thick airfoils employed in wind turbine blades.
How is the roughness modelled? How will it be defined? What range of roughness will be covered on the model training?	To be answered after specific study, Section 2.
How is the erosion modelled? How will it be defined? What range of erosion severity will be covered on the model training?	To be answered after specific study, Section 3.3.
In addition of surface condition, what other parameters will be considered?	Geometric parameters, Reynolds number and angles of attack

2 Roughness effect in transitional flows

Wind turbines blades work in variable roughness surface conditions during their operational life, new or washed blades with very low roughness levels and blades that are contaminated by insects, dirt, dust or erosion. The existence of roughness over the blade surface generates a performance loss in the airfoil aerodynamics which understanding and accurate prediction is very important for wind turbine blade designers.

The major effect of distributed roughness in the airfoil performance is to deteriorate its aerodynamic behaviour. If the rough elements are located near the leading-edge zone, roughness influences the laminar to turbulent transition process leading to early transition. In addition to promote transition, roughness also modifies the ow characteristics in fully turbulent flows. Lift decreases due to modification of the log-law velocity distribution and drag increases due to the increased shear near the surface. This results in a reduced lift to drag ratio in absolute value for all angles of attack. Boundary layer and displacement thickness also increase due to the existence of rough particles. Early stall is also expected since the increased shear due to roughness that opposes streamwise momentum dominates the separation mechanism for an equal streamwise pressure gradient. Airfoils have been designed typically to be insensitive to roughness forcing small differences between clean and tripped ow quantities.

In this section, the influence of roughness effect in transitional flow is studied. The objective is to define how real rough conditions need to be modelled and what is the influence of the roughness on transition, separation and aerodynamic performance.

It must be noted that ML algorithms might require large amount of data, therefore, there are some assumptions that need to be verified. The numerical models will be compared against experimental campaigns to perform a validation.

The LEES (Leading-edge Erosion Study) project (Maniaci & White, 2022) provided aerodynamic performance data using wind-tunnel measurements of representative inboard and outboard blade sections contaminated with various types and levels of roughness and leading-edge erosion. Results include aerodynamic load coefficients and measurements of laminar-to-turbulent transition location as functions of Reynolds number and angle of attack for various roughness configurations. The airfoils tested were an 18%-thick NACA 63-418 and a 24%-thick S814. Chord based Reynolds numbers from 1.6 to 4 million were tested. Randomly distributed additive roughness characteristic of insect carcasses was added to each airfoil. Surface area coverage between 3% and 15% and several roughness heights were tested. Measurements at the same conditions using trip-tape were also made to assess the extent to which trip-tape captures distributed roughness effects.

It is required to select and adequate turbulence model to perform the simulations. A comparison between two modelling approaches has been made. In order to alleviate the computational cost, a fully turbulent modelling ($k\Omega - SST$) is compared against a transitional model. It is considered that roughness induces a transition to turbulent behaviour closer to the leading-edge and therefore, for the sake of reducing computational cost, assuming a fully turbulent flow is justified.

2.1 Modelling description

A computational mesh generated by IWES has been employed by both IWES and CENER in order to reduce the uncertainties. It has been generated with the tool Construct2D, a grid generator designed to created 2D grids for CFD computations on airfoils. The only required input file is the set of coordinates defining the airfoil geometry, using the same format as XFoil, the well-known vortex-panel code for airfoil analysis. By means of the hyperbolic grid generation high-quality grids are obtained in a fast and accurate way. CENER has also performed computations with XFoil to assess the suitability of the tool to generate the datasets required to train the model.

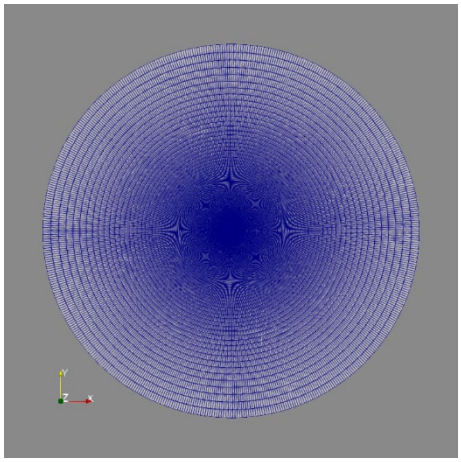

(a) Computational domain.

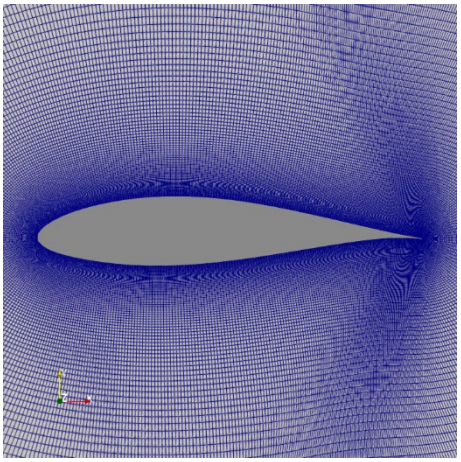

(b) Close view of the NACA63-418 airfoil.

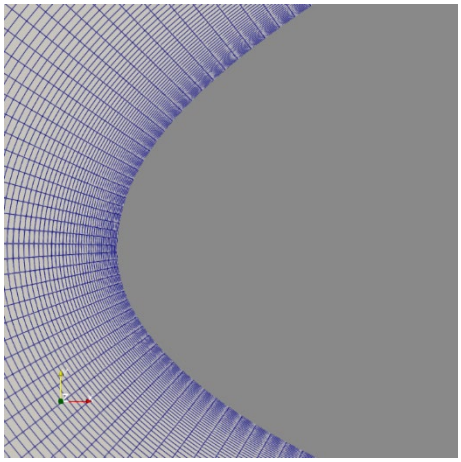

(c) Detail of the leading edge mesh.

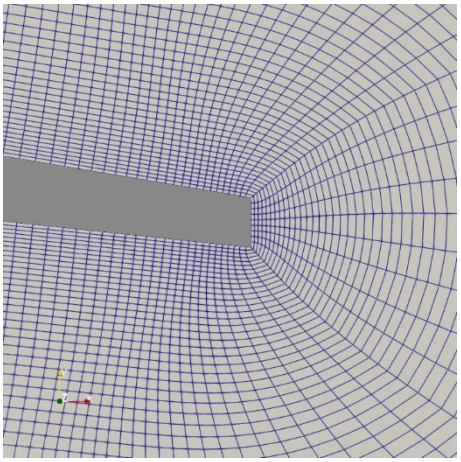

(d) Detail of the trailing edge mesh.

Figure 1 Computational mesh employed for the 2D simulations. An O-grid topology has been employed respecting the blunt trailing edge.

Figure 1 shows the computational domain (a), a view of the mesh close to the airfoil (b), and details of the mesh at the leading-edge (c) and the trailing-edge (d). The characteristics of the mesh are summarized in Table 2.

Table 2. Mesh characteristics.

Feature	Value
Chord	1 m
Far field location	310 chords in radial direction
First element height	1.67×10^{-4} m
Surface discretization	512 elements
Trailing edge gap discretization	9 elements
Total number of elements	130560

2.1.1.1 Clean condition comparison

A comparison between three modelling approaches has been made. The surface condition considered on the model is clean, i.e., no surface degradation is considered. The modelling approaches are described below:

1. LEES experimental data
2. IWES modelling, CFD simulation results considering transitional flow, $k\Omega SST - LM$.
3. CENER modelling, CFD simulation results considering transitional flow, $k\Omega SST - LM$.

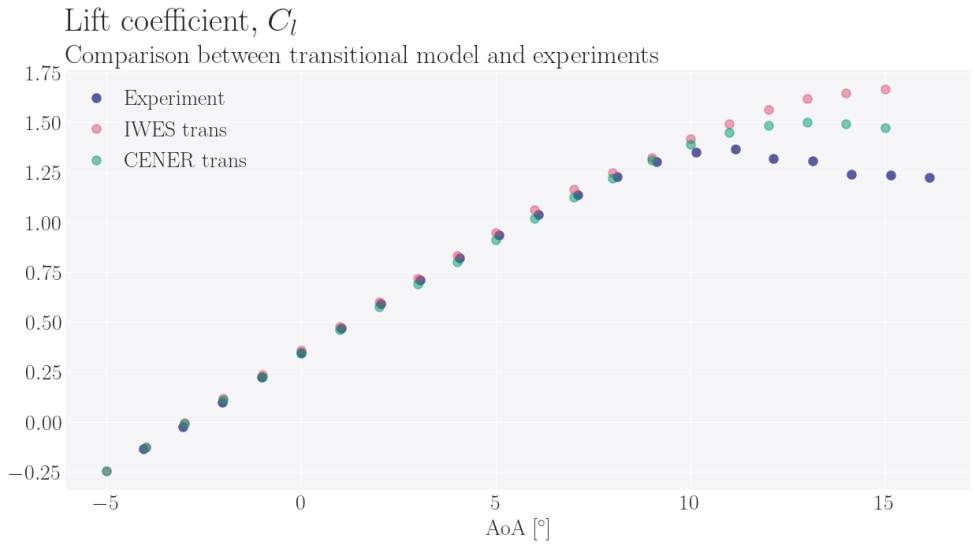

Figure 2. Lift coefficient comparison between two transitional CFD and the experimental data for the NACA 63-418 airfoil in clean status.

As shown in Figure 2, there is a good agreement between the simulations and the experimental campaign regarding lift coefficient. Deviations from the experimental data start close to the stall region, at angles of attack higher than 10°. The differences between the CFD results are caused by the differences between numerical schemes (the same mesh is used). While the lift obtained by CENER presents a maximum at 13°, IWES simulations do not achieve a maximum at the considered angles of attack. This results in higher deviation from experimental lift values. If the drag coefficient is compared, Figure 3, CENER modelling clearly overestimates the experimental data at angles lower than 10°. This is not the case of IWES setup, which results in a good agreement with experimental values at those angles. Nevertheless, the behaviour is swept at higher angles of attack where IWES deviates from the experimental values of drag coefficient. It must be noted that at the angle of attack of 10° is where the stall appears in the experimental data.

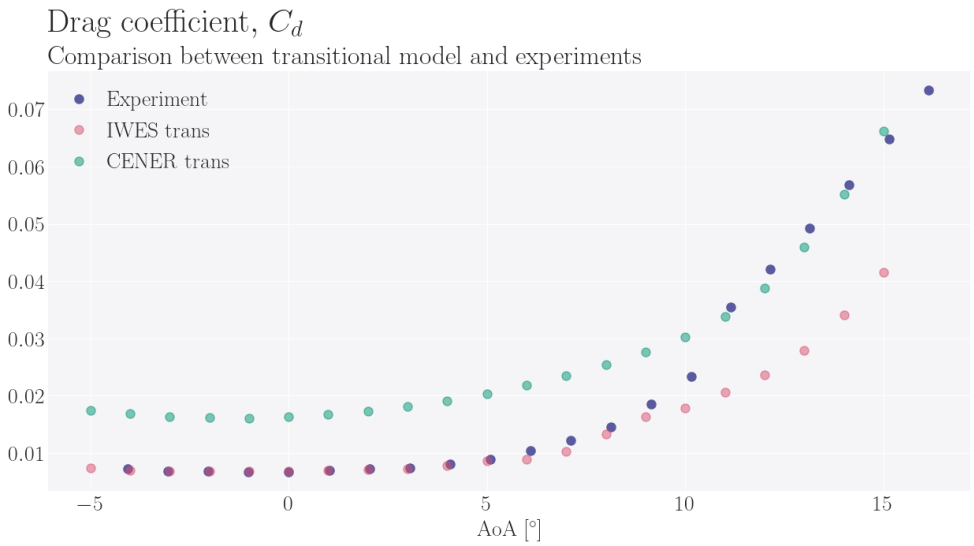

Figure 3 Comparison of the drag coefficient between two CFD models and experimental data for the NACA 63-418 airfoil in clean status.

2.1.1.2 Rough condition comparison

Figure 2 and Figure 3 showed deviations close to the stall region. Figure 4 presents the lift coefficient obtained for the rough case described at the beginning of this section: NACA63-418 airfoil at Reynolds 3 million with 200 micron distributed roughness over the 3% of the upper side and 15% on lower side. Experimental values are depicted in blue dots. Two CFD results are also shown in the figure. Pink dots represent the values obtained by IWES considering the flow as fully turbulent. The difference with regard to the experimental values is reduced when roughness is considered, and good agreement is now obtained even at the stall region. If the flow is transitional, green dots, the difference between experimental and simulation results are also reduced.

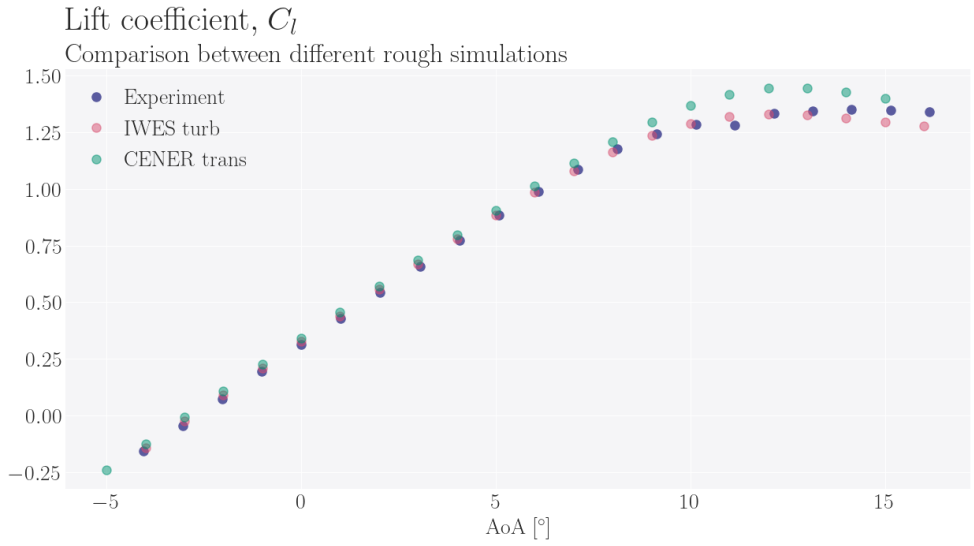

Figure 4 Lift coefficient comparison between experimental data (blue), fully turbulent flow (IWES) and transitional flow (CENER). The NACA 63-418 airfoil has been analysed in rough condition.

Nevertheless, a better agreement is obtained when fully turbulent flow is considered. Therefore, it is not justified the increase in computational cost of the transitional model if more accurate results are obtained considering the flow fully turbulent. This is also the case of the drag coefficient, Figure 5. The transitional approach overestimates the drag at all the angles of attack considered while the fully

turbulent approach results in great agreement with the experimental data. Only at the three higher angles of attack an overestimation is observed. It can be concluded that the fully turbulent approach results in better characterization of the aerodynamic performance of an airfoil suffering from leading edge roughness.

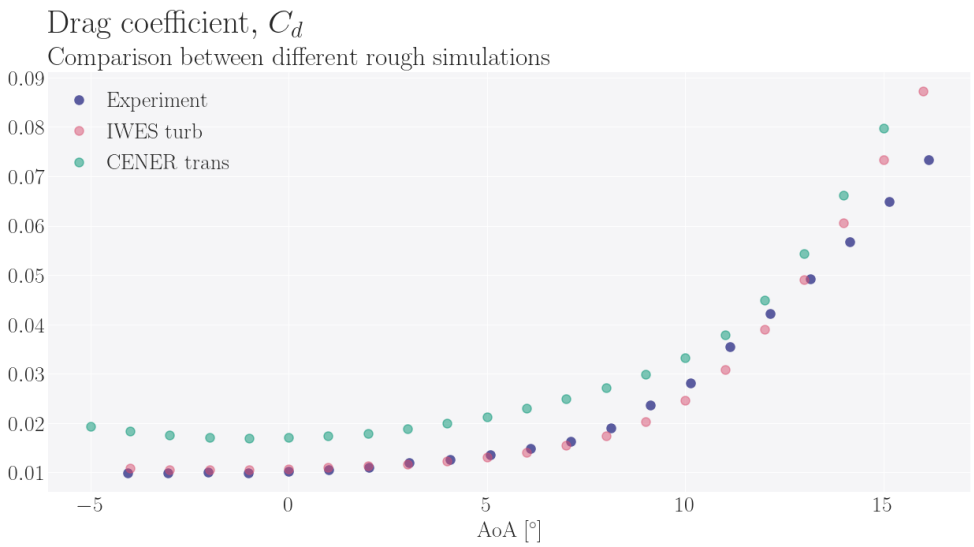

Figure 5 Drag coefficient comparison between experimental data (blue), fully turbulent flow (IWES) and transitional flow (CENER). The NACA 63-418 airfoil has been analysed in rough condition.

2.1.1.3 Comparison between panel codes and CFD simulations

In addition, the suitability of XFoil to determine the aerodynamic coefficients under rough conditions is assessed. Two sets of simulations have been carried. First of all, the clean status is considered. The turbulence intensity of the wind tunnel where the experimental campaign was performed is 0.75% which results in an N_{crit} of 3.383. Figure 6 compares the aerodynamic coefficients from three different sources: experimental values (blue dots), transitional CFD modelling (pink dots) and XFoil modelling (green dots). The left figure shows the lift coefficient while the right one presents the drag coefficient. It is remarkable the agreement between the CFD and XFoil results at the angles of attack considered. Nevertheless, both modelling approaches deviate from the experimental values at angles of attack higher than 10°. The computational cost reduction that the employment of XFoil would produce is supported by this agreement shown. Even though, it is required to test XFOIL performance on rough conditions. It is considered that the roughness will provoke an early transition to turbulent flow. To reproduce this behaviour the value of N_{crit} is set to 0.1, resulting in trainsition to turbulent close to the leading edge. Figure 7 represents, following the same convention as in Figure 6, the comparison between experiments, fully turbulent CFD and XFoil simulations. Good agreement with experimental and CFD data is achieved at AoAs lower than 6° for both the lift and drag coefficient. Nevertheless, great deviations are observed at higher AoAs. Moreover, it is not possible to control the severity of the roughness with XFoill v6.99.

Even though XFoil has a very reduced computational cost its employment for the generation of the aerodynamic dataset is discarded beacuse with XFoil v6.99 it is not possible to model appropriately the leading-edge roughness or the erosion.

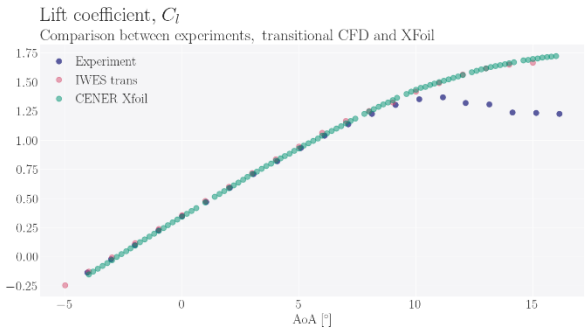

a) Lift coefficient

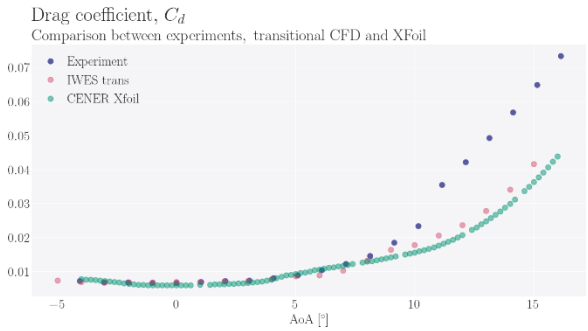

b) Drag coefficient

Figure 6 Comparison between the experimental values (blue dots) and the numerical results of the NACA 63-418 airfoil under clean conditions. Two models are compared IWES transitional CFD (pink dots) and XFOIL computations performed by CENER (green dots). On the left, Figure 6a, the lift coefficient is shown while the drag coefficient is represented on the right, Figure 6b.

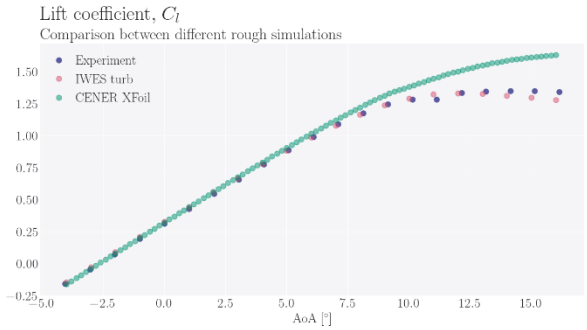

a) Lift coefficient

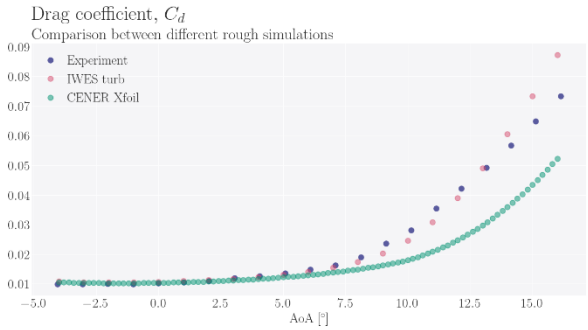

b) Drag coefficient

Figure 7 Comparison between the experimental values (blue dots) and the numerical results of the NACA 63-418 airfoil under rough conditions. Two models are compared IWES fully turbulent CFD (pink dots) and XFOIL computations performed by CENER (green dots). On the left, Figure 6a, the lift curve is shown while the drag curve is represented on the right, Figure 6b.

2.2 Roughness modelling

The rough simulations previously shown employ the Cebeci and Bradshaw roughness model (Cebeci & Bradshaw, 1997). This model is based in empirical correlations that modify the turbulent boundary layer equations to take into account rough elements on the surface of the airfoil. It adjusts the turbulent viscosity and eddy diffusivity in the near-wall region. As shown in the comparison (Figure 4 and Figure 5), a good agreement between numerical and experimental values is obtained with this model and therefore it will be employed on the dataset generation.

The roughness is, then modelled by the following parameters:

- Equivalent sand-grain height, h_r. The relationship between the roughness height measured on a blade inspection and the equivalent sand-grain height is the Cousteix relationship (Cousteix, 1989).
- Extension of the distributed roughness. The area where the roughness is placed needs to be specified. In this work, it is considered that the roughness is located at the leading edge. Therefore, two values are needed, the extension of the roughness in the upper surface of the airfoil, u_r, and the extension on the lower surface, l_r.

These three parameters are depicted on Figure 8. The figure shows the extension of the roughness area at the lower and the upper sides of the airfoil as well as the physical interpretation of the parameters.

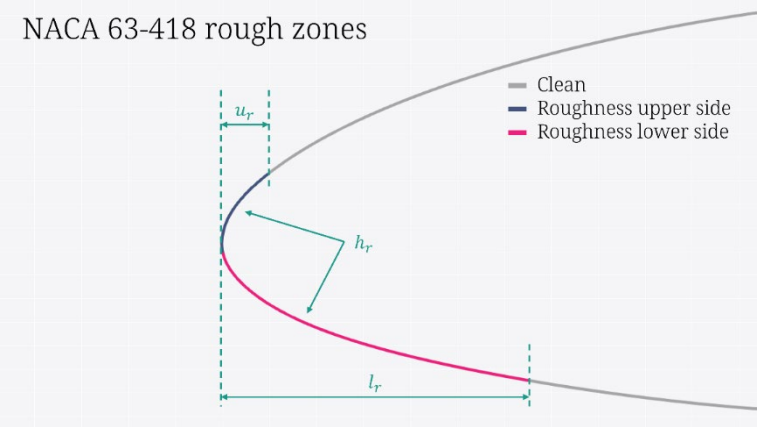

Figure 8. The roughness parameters employed on the NACA 63-418 rough simulations, Figures 4 and 5, are $h_r = 200\ \mu m$, $u_r = 0.03$ and $l_r = 0.15$.

2.3 Conclusions

The main conclusions of the presented study are:

- The tool Construct2D will be employed for grid generation as it generates high-quality and reliable meshes employing as input the airfoil geometry in XFoil format.
- Fully turbulent approach is suitable for the data generation required to train and validate the ML models.
- The modelling approaches will be further validated against wind tunnel experimental campaigns that will be carried in AIRE WP6 as well as blade inspections after a calima event.
- Due to the deviations between XFoil and CFD simulations, XFoil will not be employed to generate the aerodynamic dataset. Moreover, it is not possible to model erosion in XFoil and, in order to reduce uncertainties, only CFD results will be employed.

3 Blade damage during service life

3.1 OREC blade inspections

The Offshore Renewable Energy (ORE) Catapult, as part of the AIRE 3.3 project, has been tasked with providing representative changes in Annual Energy Production (AEP) for their reference experimental wind turbine when blade damage is reported. This assessment can be conducted both theoretically, using estimates, and experimentally, through the analysis of SCADA data and power curves. This report aims to evaluate the accuracy of both methods, detail their uncertainties, and discuss the practical implications of estimating AEP losses.

Located off the Fife coast in Scotland, ORE Catapult's Levenmouth Demonstration Turbine (LDT) is the world's most advanced, open-access offshore wind turbine dedicated to R&D, shown in Figure 1. Unique among offshore wind testing facilities, the towering 7MW machine plays host to some of the industry's most exciting innovations for testing and validation.

Figure 9. ORE Catapult's ' 7MW offshore wind turbine at Levenmouth.

Since 2021, LDT has been the focus of various leading-edge protection (LEP) studies. This has included characterisation of LEP's in the rain erosion test (RET) rig and further assessment of in-situ performance over the years of installation on LDT using drone inspections. Figure 10 provides an example of a drone image showing the leading edge with instances of erosion. Such high-detail imagery allows for zooming in on points of interest, supporting the assessment of the erosion stage (category) and position, which are crucial inputs for modelling and comparison with RET results.

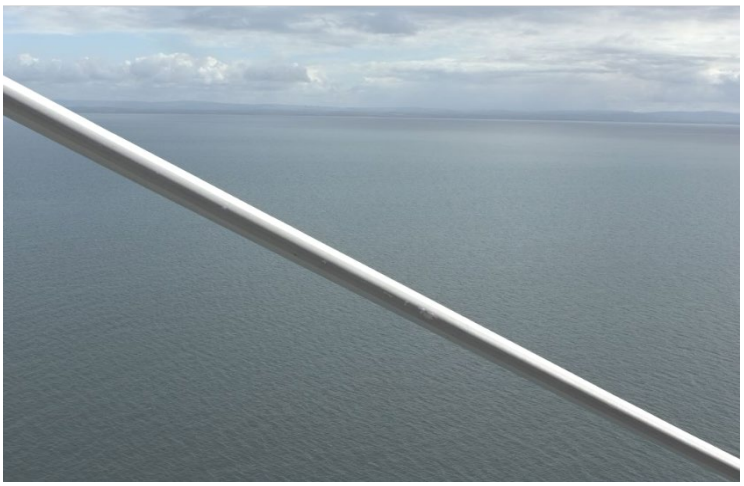

Figure 10. Example image of LDT blade with erosion

Through these initiatives, ORE Catapult aims to advance understanding and improve methodologies for estimating and mitigating AEP losses due to blade damage, thereby enhancing the reliability and efficiency of wind energy production.

3.1.1 Methodology for Evaluating Erosion Power Performance Losses

This study will compare and evaluate the effectiveness of estimated power loss from leading edge erosion (LEE) or generally leading-edge roughness (LER), against actual power loss. DTU's aerodynamic tool, SALT, is used to predict LER losses, using defect characterisation from drone inspection as inputs. SCADA data from LDT will reveal actual losses from LER and a discussion will explore the validity of this method.

3.1.1.1 SALT Tool

As described by DTU: *SALT is a fast BEM-based tool to predict the loss in annual energy production for a wind turbine, due to aerodynamic deterioration of different spanwise sections of its blades. It relies on a simplified BEM model to compute the aerodynamic performance of the rotor and perturbs the sectional lift coefficient and lift-to-drag ratio to assess the losses.*

This calculation tool is initially made to predict the annual aerodynamic energy loss relative to the starting point.

The motivation to formulate this model is that wind turbine owners neither have much information about the wind turbine nor information about the real surface conditions of the blades - apart from photos from inspections.

Therefore, this tool only requires a few parameters: Rated power, rotor radius, air density, Weibull parameters A and k and categories describing the surface conditions of each blade. The remaining parameters required to describe the rotor operation is assumed.

Figure 11, a screen grab from the SALT tool displays operational and environmental inputs for the LDT study. Environmental inputs include the Weibull parameter (c) of 6.67 m/s, which is obtained from LDT's anemometers, and the Weibull coefficient (k) remains at the standard value of 2. Operational inputs consist of the rated power of 7 MW, blade radius of 85.6 m, constant air density of 1.223 kg/m^3, maximum tip speed of 95 m/s derived from turbine rpm data and radius, a standard drive train efficiency of 0.94, and standard aerofoil cl/cd values.

Power rated=	7000	kW
Radius=	85.6	m
B(no of blades)=	3	
Ro=	1.225	kg/m^3
Max tip speed=	95.0	m/s
TSRopt	8.00	-
A=	6.67	m/s
Vave (Rayleigh)=	5.91	m/s
k=	2	-
P_specific=	304.1	W/m^2
CP_max=	0.483	-
V_rated=	10.09	m/s
Drivetrain-eff.=	0.94	-
cl_design=	1.13	-
cl/cd_clean,70	110	-
cl/cd_clean,30	78	-
cl/cd_clean,0	6	-
Start of LEP =	62	m

Figure 11. Operational and environmental inputs into SALT to compute theoretical clean power performance and theoretical LER power performance (screen grab from SALT)

The complexity and variety of erosion damage presents significant challenges for the industry, with many different categorization systems and a lack of standardisation. Addressing this issue, IEA Wind Task 46 WP 3 has developed a comprehensive classification system based on a range of images, as detailed in their findings, Task 46 Results | IEA Wind TCP (iea-wind.org). Despite this, different organisations use varying definitions. For instance, DTU's SALT tool categorises erosion based on sandpaper roughness. While ORE Catapult adheres generally to the IEA Wind Task 46 WP 3 classification, variations still exist depending on the composition and type of the LEP system. To streamline this process for the LDT study, simplifications are made to align with these classifications.

- Smaller instances of erosion incubation are challenging to detect through drone images, the LDT blades contain significant amounts of dirt and the LEP's are applied using rope access hence are not completely aerodynamically smooth. Consequently, for this study, it is assumed that any area of the blade without visible defects of at least 50x50 mm is classified as category B.
- Incubation (50x50 mm) – as defined by ORE Catapult in Figure 13, is equivalent to category C.
- Smaller defects such as bubbling of the product as defined by ORE Catapult in Figure 13, is equivalent to category D.
- Exposure of filler as defined by ORE Catapult in Figure 13, is equivalent to category E.
- Damage to the composite as defined by ORE Catapult in Figure 13, is also equivalent to category E since there are no further categories available in the SALT tool.

Categories	
a	A new and clean blade section with almost no leading edge surface damages or imperfections
b	A blade section with small damages at the leading edge and with a surface roughness smaller than P400
c	A blade section with a leading edge with a surface corresponding to sandpaper P400
d	A blade section with a leading edge with a surface corresponding to sandpaper P40 or with a cavity with depth 0.3% time the chord length
e	A blade section with a leading edge with surface damages more severe than sandpaper P40 or somewhat deeper than 0.3% times the chord length

Figure 12. Categories used to describe the erosion states on the wind turbine blade (screen grab from SALT)

Figure 13. Erosion categories used by ORE Catapult following closely IEA Wind Task 46's definitions. Left: Incubation, Left middle: Bubbling/other minor defects, right middle: Filler exposure, right: composite exposure

Figure 14, another screen grab from SALT tool, displays the complete defect characterisation as inputs into the tool. The occurrences of these defects are from approximately 30/08/2023 to the present. During this time, blade A experienced stripping from 85 to 75 m due to LEP damage. Blade B showed significant defect-driven erosion, characterised by random erosion points and no clear erosion front typically observed in LEP gelcoats. Blade C also experienced localised and defect-driven erosion similar to blade B, but this was only confined to the tip section.

r	Blade A - No LEP past Category	Blade B Category	Blade C Category
62.00	b	b	b
62.66	b	b	b
63.31	b	b	b
63.97	b	b	b
64.62	c	b	b
65.28	c	b	b
65.93	c	b	b
66.59	c	b	b
67.24	c	b	b
67.90	c	d	b
68.56	c	d	b
69.21	c	b	b
69.87	c	d	b
70.52	c	d	b
71.18	c	d	b
71.83	c	e	b
72.49	c	b	b
73.14	c	b	b
73.80	c	b	b
74.46	c	b	b
75.11	b	b	b
75.77	b	b	b
76.42	b	b	b
77.08	b	b	b
77.73	b	b	b
78.39	b	b	b
79.04	b	b	b
79.70	b	b	b
80.36	b	d	b
81.01	b	d	b
81.67	b	b	b
82.32	b	b	b
82.98	b	b	b
83.63	b	e	e
84.29	b	d	e
84.94	b	c	e
85.60			

Figure 14. Blade A-C erosion states along the LEP length of 62m to 85.6m at the tip (screen grab from SALT)

3.1.1.2 Power Curve generation from LDT SCADA

The methodology for deriving the power curve based on real LDT SCADA data has followed the IEC 61400-12-1 standard. However, due to the nature of LDT, its use as a demonstrator turbine and the significant period of curtailment, hours out of operation and operation in experimental states, there is a significant amount of further data filtering required, to obtain a power curve that represents LDT at optimal performance. *Figure 15* displays the original, unfiltered data for the dates of the analysed erosion damage and when the turbine was expected to be free of erosion close to its installation in 2017. Specifically, LER true data was collected from 01/07/23 to 01/11/23, and clean true data was collected close to the installation of LDT from 01/04/17 to 01/08/17. These dates were chosen because the turbine experienced significant downtime after 08/17, so the same time of year could not be used.

As anticipated, the data reveals significant data points below the power curve, rendering the calculated power curve unusable. Wind speeds are recorded from a hub height anemometer at the onsite met mast, the uncertainty of which will be discussed in the results section, and power is obtained from the LDT SCADA system.

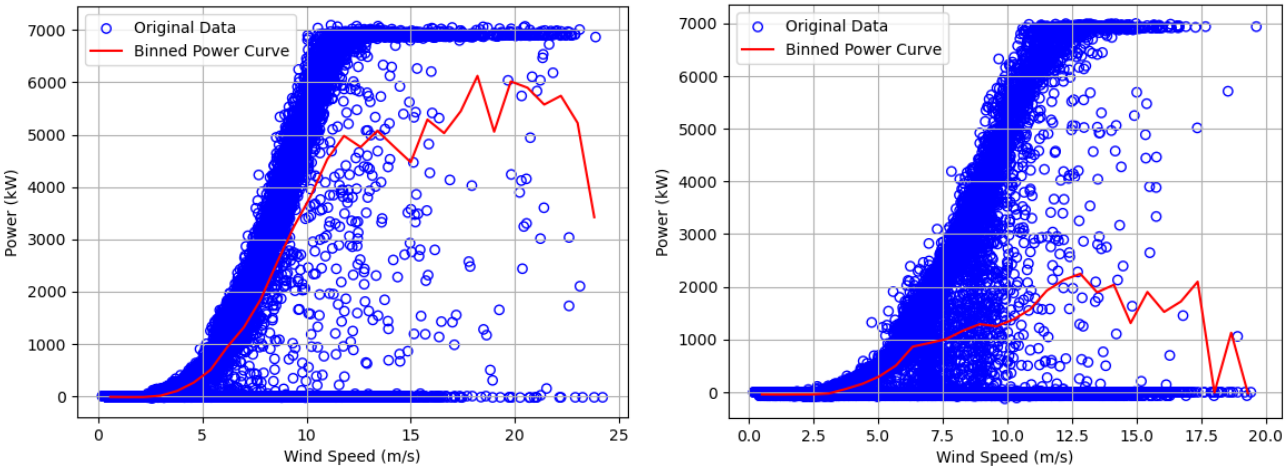

Figure 15. Power curve of LDT from the dates left (LER): 01/07/23 - 01/11/23, right (clean): 01/04/17 – 01/08/17, whilst erosion was at the state entered into SALT, original data with no filtering

Further filtering of the power curve has been achieved using the following conditions:

- Turbulence intensity between 0.04 and 1, filtering any points of non-optimal power generation.
- Nacelle position between 210° and 260°, determined from the LDT wind rose to be the prominent wind direction, filtering any points of non-optimal power generation.
- Yaw misalignment between 0.1° and -0.1°, filtering any points of non-optimal power generation.
- Rotor RPM between 0.4 and 1.2 RPM, corresponding with cut-in wind speed and cut-out but also filtering any duration that the turbine is out of operation.
- Blade pitch between -1° and 16°, determined from a histogram of the data, filtering any points of non-optimal power generation.
- Wind speed between 3 and 25 m/s, also filtering any duration that the turbine is out of operation.

Figure 16 displays the filtered data for both LER dates (right) and dates when the turbine was expected to be free of erosion close to its installation in 2017.

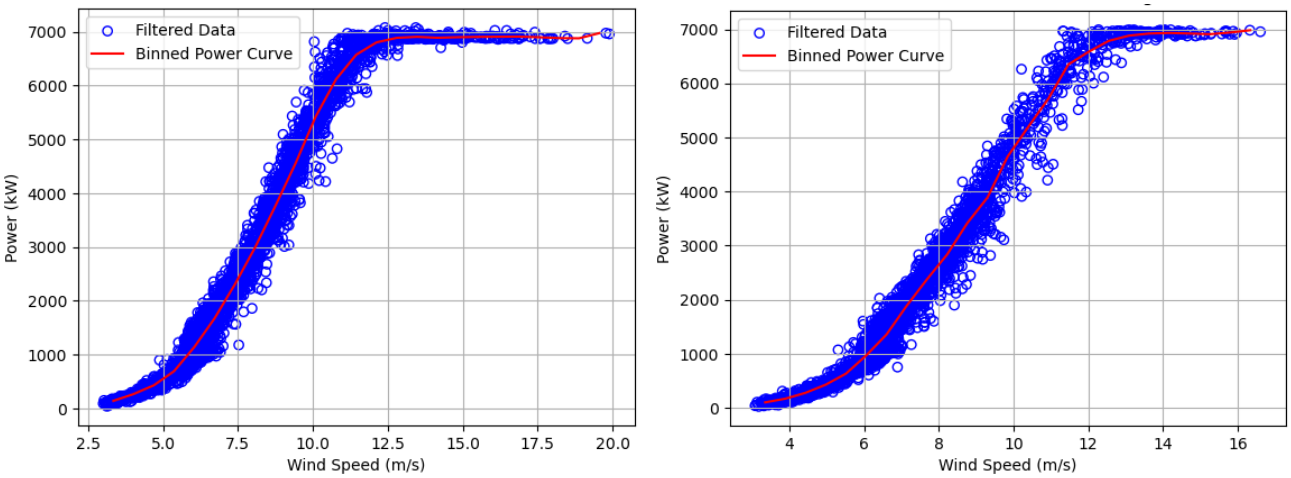

Figure 16. Power curve of LDT from the dates left (LER): 01/07/23 - 01/11/23, right (clean): 01/04/17 – 01/08/17, whilst erosion was at the state entered into SALT, filtered data

3.1.2 Results and Discussion of Erosion Power Performance Losses

Figure 17, a screen grab from the SALT tool, shows the predicted LER AEP loss is 1.24%. Although this is significant for operators, it is lower than most reported LER AEP losses in literature. This can be attributed to two factors. Firstly, there has historically been an overestimation of the effects of LER. Secondly, the LEPs on LDT do not show a typical erosion front. Unlike traditional gel coats, which exhibit

an erosion front from tip to root, the newer coatings trialled on LDT demonstrate defect-driven erosion. This means that small inconsistencies in the material or application procedures lead to erosion that does not follow the typical pattern. Instead of growing towards the root, the individual defects grow into the blade composite.

AEPloss=	1.24 %	
AEPclean=	18.722	GWh
AEPler=	18.489	GWh
Delta(AEP)=	232.4	MWh

Figure 17. Maximum AEP loss during LER derived by SALT tool

Power Curve Comparison and Analysis

The theoretically derived power curves for LER and clean states using the SALT tool were compared against the actual power curves derived from LDT SCADA data for the same states. The results are shown in *Figure 18*.

Comparison of SALT Tool Curves:

The SALT tool's results indicate minimal differences between the LER and clean states. The LER power curve slightly trails behind the clean power curve, suggesting a minor impact of leading-edge roughness on the turbine's aerodynamic performance in the theoretical model. This minimal lag indicates that, under the idealised conditions simulated by the SALT tool, the presence of LER causes only a slight decrease in power output.

Comparison of True Data Curves:

In contrast, the true data curves derived from SCADA data exhibit an unexpected pattern: the LER state appears to generate more power than the clean state. This is contrary to aerodynamic principles and literature, as LER typically increases drag and reduces lift, leading to lower power output. This discrepancy highlights potential uncertainties in the data, likely due to the sensitivity of the SCADA-based power curve generation methodology to small uncertainties and errors in measurement.

Accuracy and Limitations of Anemometers:

According to IEC 61400-12-1 standards, anemometers are deemed sufficient for wind speed measurement. However, they lack the necessary fidelity to accurately assess small AEP losses, such as the 1.24% reduction attributed to LER. The precision required to detect such minor losses is beyond the capability of traditional anemometer-based measurements, necessitating the exploration of more accurate methods such as lidar data, which offers higher resolution and accuracy in wind speed and direction measurements.

Impact of Vortex Generators:

During the period when LER data was collected, LDT conducted trials with vortex generators. These devices are designed to improve aerodynamic performance by delaying flow separation on the blade surfaces, thereby enhancing lift and reducing drag. The expected gain in AEP from using vortex generators is approximately 1-3%. This potential increase could explain why the LER power curve is observed to be higher than the clean power curve in the true data, as the benefits of the vortex generators might be masking the negative effects of LER.

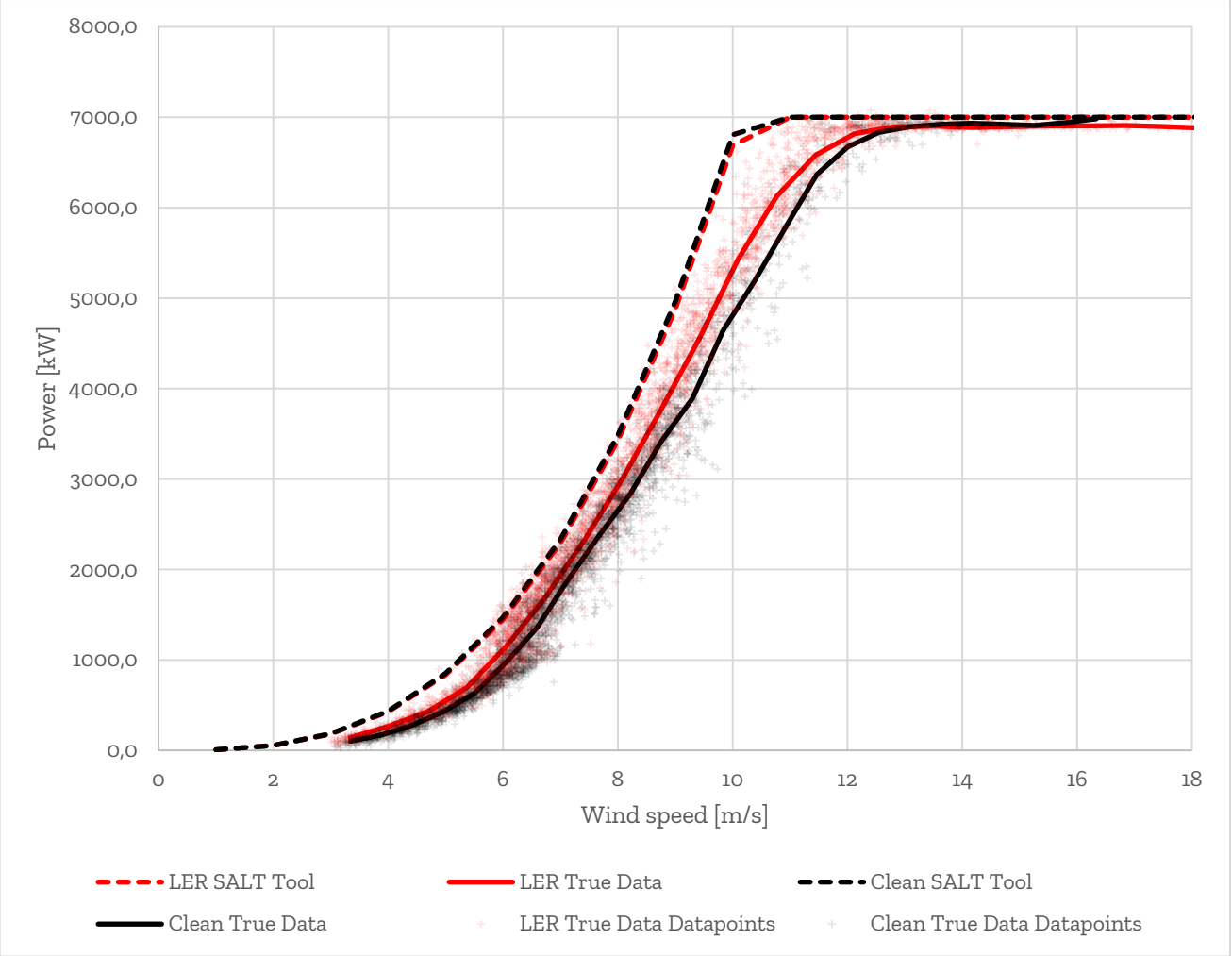

Figure 18. Results: SALT results plotted with in-situ results

3.1.3 Conclusion

It is concluded that small AEP losses due to blade erosion cannot be accurately monitored using SCADA-based power curve analysis, given the uncertainty in power measurements. The discrepancies between the SALT tool and SCADA-derived power curves can be attributed to the idealised conditions assumed by the SALT tool, which generally align with the outermost data points of the true data.

Despite the limitations of SCADA data in erosion monitoring, the SALT tool remains valuable for operational and maintenance (O&M) teams. If inspection images can be labelled for erosion defects and automatically integrated into the SALT tool, it can provide estimations of AEP losses due to LER. Tracking changes in these values over multiple inspections can guide decision-making based on tangible monetary losses rather than only drone inspection images. It is vitally important that the categorisation of LER remains constant throughout this process.

Future work should focus on integrating higher fidelity measurement tools, such as lidar, into the power curve analysis process to improve accuracy in detecting small performance losses. Additionally, further validation of the SALT tool with real-world data and more modern LEPs under various operational conditions will help refine its predictive accuracy and enhance its utility for O&M decision-making.

3.2 Alaiz blade inspections

A Siemens-Gamesa G10X-132 wind turbine at the CENER's Experimental Wind Farm was inspected with drone imaging to analyse the blade status. This WT has a rated power of 5MW with a hub height of 117.5 m and 132 m of diameter. The drone inspection was carried out in February by the company ALERION. On their report, they categorize the blade damages as presented in Figure 19.

SEVERITY	CHARACTERISTICS	
1	Description	Minor variances from supply specifications but within acceptable (or industry typical) tolerances; may affect the appearance of the blade or blade feature. Though minor, can be useful to identify as position references, or for blade identification.
	Potential for growth	None expected.
	Impact to aerodynamics	None expected.
	Impact to life	None expected.
2	Description	Minor damage or defects that exceed supply specification acceptance criteria. Multiple cosmetic findings and/or a single major cosmetic finding that are damage, defects, or former repairs. Findings exceed tolerances of supply conditions or industry typical manufacturing variability. Repairs of more severe damage or defects can be recategorized to category 2 upon review of repair.
	Potential for growth	Not likely but may accelerate leading edge erosion when located on the leading edge, additionally may leave laminate or bond lines exposed to environmental degradation. Generally, 100 percent growth in size or severity pushes finding into next category.
	Impact to aerodynamics	May have minor impact to aerodynamics depending on details, though beyond what could reasonably be measured.
	Impact to life	None expected.
3	Description	Moderate to minor structural damage or minor manufacturing defects in non-critical areas. Features are moderately out of compliance with supply conditions and/or below minimum typical industry practice. May present as surface indications when in fact there is damage to the underlying structural laminate. Internal inspection may be needed to determine the extent of the finding. May be particularly challenging to assess criticality due to lack of design data such as load margins. Findings may be category 3 when category 4 actions seem too drastic and category 2 is not appropriate, because there is a slight risk of loss of structural capability.
	Potential for growth	Likely to increase in size or extent over time and become more severe. Growth in size or severity by 50 percent or more is likely to push finding into next category.
	Impact to aerodynamics	May have an impact to aerodynamics depending on details.
	Impact to life	Life is expected to be reduced without some other measures such as monitoring or repair or engineering evaluation (in the case where there is sufficient margin).
4	Description	Significant damage or defects that have notable impact to structural capability and/or aerodynamic performance.
	Potential for growth	Likely to increase in size or extent over time and become more severe. Growth in size or severity of 10-50 percent is likely to push finding into next category.
	Impact to aerodynamics	Likely to have an impact to aerodynamics depending on details.
	Impact to life	High confidence the blade will not achieve intended life.
5	Description	Severe degree of damage or defect such that there is a high risk of imminent failure.
	Potential for growth	Likely to rapidly increase in size or extent.
	Impact to aerodynamics	Likely to have an impact to aerodynamics depending on details.
	Impact to life	The blade is expected to fail within a short period of time if operated.

Figure 19 Blade condition categorization from AILERON report.

A total number of 56 damages were found as summarized on Figure 20. Blades A and B have been found to have similar damages while blade C is the one with the most harmful damage of category 3.

		Damages Category				
WIND TURBINE	BLADE	1	2	3	4	5
T0	A	12	9	0	0	0
	B	12	8	0	0	0
	C	11	3	1	0	0
	Total	35	20	1	0	0

Figure 20 Summary of the damages found on the wind turbine.

A 60.71 % of the damages are classified as dirt (category 1). Figure 21 shows an example of a damage categorized as dirt. Of them, the 44% were located in the root of the blade but only 14.7 % were in the leading edge.

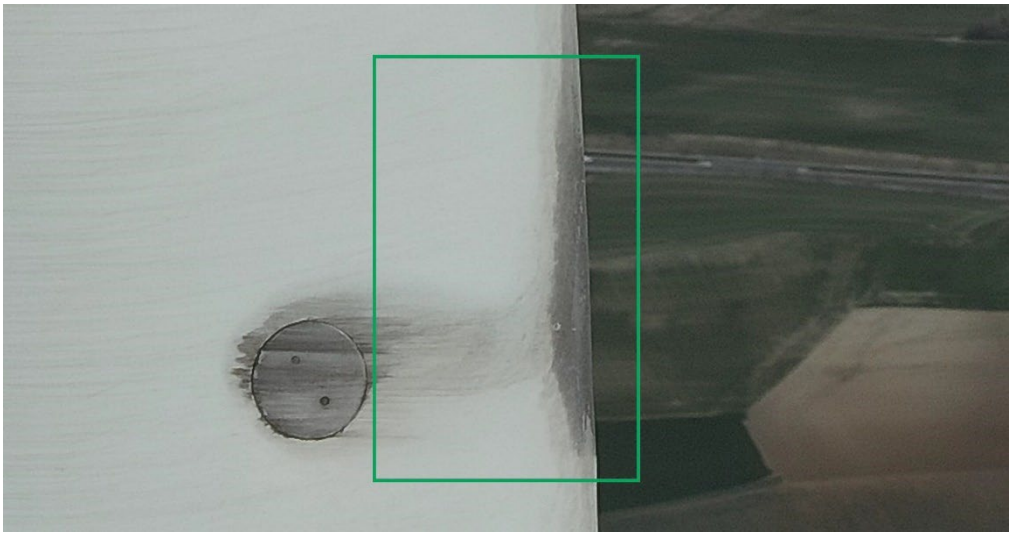

Figure 21 Dirt found at the 90% of the span on blade C. The dirt is located at the trailing edge. Dirt is highlighted with a green rectangle.

A 30.36% of the damages are reported to be pitting (category 2). To determine the pitting influence on the aerodynamic performance of the wind turbine it should be needed a more thorough blade examination. Only a 17% of the pitting was found on the leading edge of the blade while 82% was found at the trailing edge. For instance, two examples of pitting are shown in Figure 22. On Figure 22 (a) the pitting is located in the leading edge while (b) shows the pitting at the leading edge. The drone inspection was not able to characterize the depth of the pits. 47 % of the pitting occurs at blade spans between 50% and 75% while only a 6% appear at the tip blade.

a) *Pitting located at the leading edge of blade A. Damage located at the 68% of the span.*

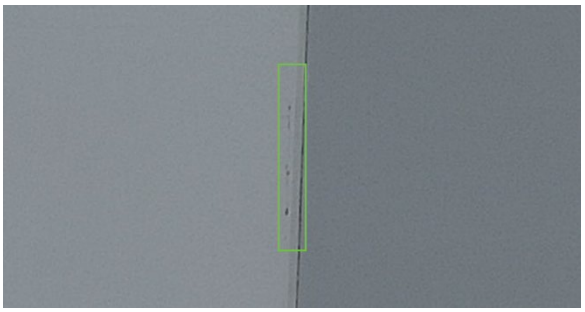

b) *Pitting located at the trailing edge of blade A. Damage located at the 42% of the span.*

Figure 22 Examples of pitting found on blade A.

In view of the results of the inspection, the blades are in a good state of preservation. Nevertheless, two damages need to be highlighted. Blade A presented erosion on the trailing edge at a section located at the 33%, Figure 23. The erosion area is 0.0353 m^2 with a maximum length of 803 mm and a minimum of

51 mm. Figure 24 shows the only category 3 damage found. It appears to be as a crack on the trailing edge of blade C. This damage is located at a blade span of 21% with a maximum length of 35 mm.

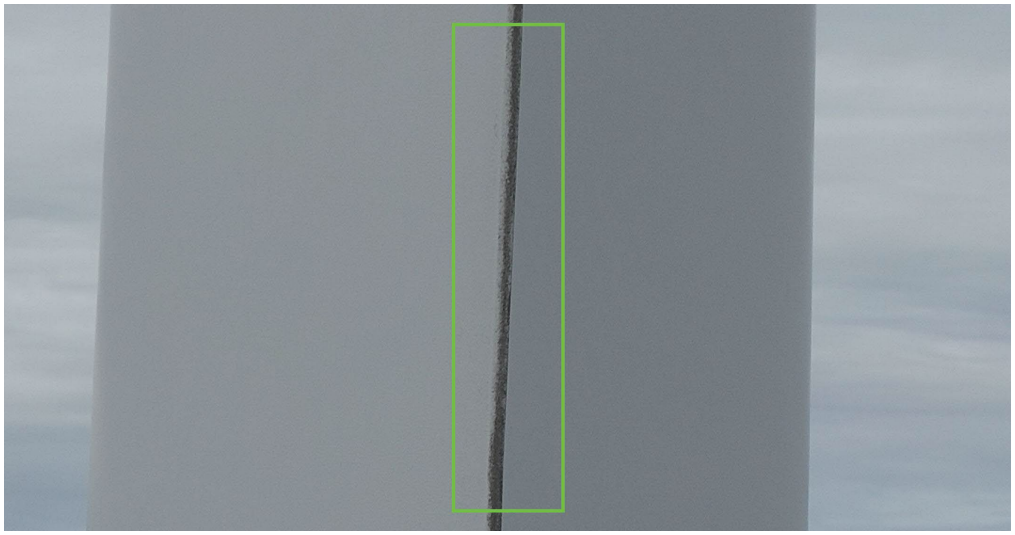

Figure 23 Erosion found on the trailing edge of blade A.

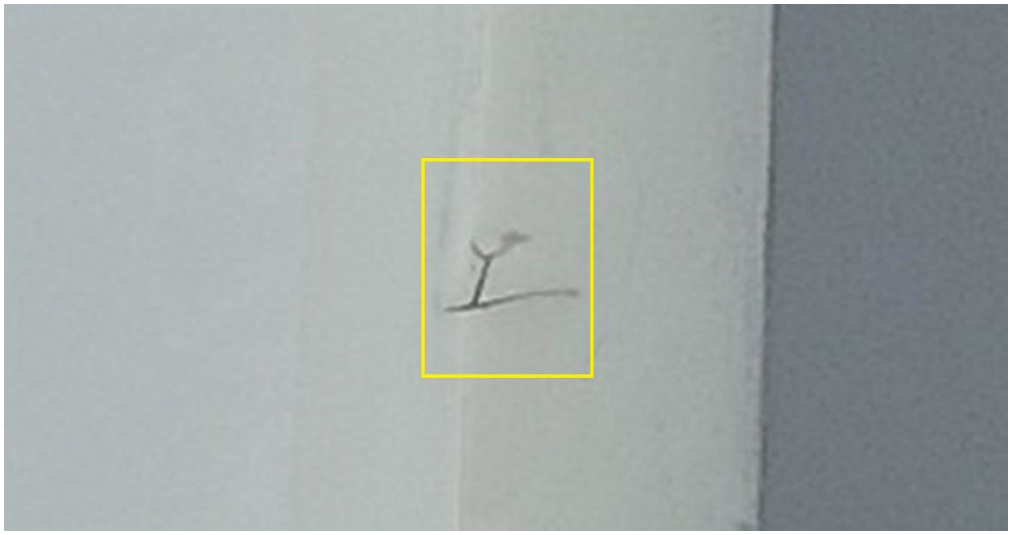

Figure 24 Category 3 damage found on the trailing edge of blade C.

Finally, Table 3 and Table 4 summarize the location and blade side at which the damages have been found.

Table 3 Damage location according to the blade span.

Location	Root (< 33%)	Internal (< 50%)	External (< 75%)	Tip (> 75%)
Damaged found (out of 56)	26.8 %	21.4%	17.9%	33.9%

Table 4 Damage location according to the blade side.

Side	Leading edge	Pressure side	Suction side	Trailing edge
Damaged found (out of 56)	17.9 %	19.6 %	26.8 %	35.7 %

It must be concluded that the information obtained from the blade inspection performed in Alaiz will help to study the dynamic evolution of erosion and dirtiness for in-service blades. In addition, 5 of the 19

most severe damages found were located at leading edge all of them at blade spans higher than 50%. The other 14 damages were located at the trailing edge with 6 of them at spans higher than 50%.

3.3 Erosion modelling

In order to model erosion, the airfoil surface needs to be modified. Erosion starts with the generation of pits, which then progresses into gouges and eventually lead to the loss of top coat. On (Saenz, Méndez-López, & Muñoz, 2022), erosion damage is grouped into two typologies. Typology 1 includes pits and gouges while Typology 2 includes different degrees of extended damage on the leading edge. On the present analysis, only Typology 2 is considered which is the most harmful of all those considered in (Saenz, Méndez-López, & Muñoz, 2022)

In Figure 12, erosion is considered as a cavity and its severity is divided in two ranges: those representing a loss of material lower than a 0.3 % of the airfoil chord and those higher than 0.3%. These categories are considered to be uniform along the leading edge. Therefore, three parameters are needed to model the material loss:

- Affected lengths on the upper and lower surfaces of the airfoil, u_e and l_e.
- The percentage of the chord corresponding to the material loss that is going to be considered, h_e.

As said, the difference between the clean and eroded model employed to analyse the aerodynamic performance of an airfoil is the modification of the leading edge. In order to do so, a constant loss of material is considered, of height h_e over the specified surfaces. The modification of the airfoil geometry is performed as follows:

- Points representing the start and end of the affected surfaces are included defined by interpolation of their position in the chord direction.
- The tangential and normal directions at the original points are computed by means of finite differencing.
- The so-called eroded points, that represent the eroded geometry, are defined by the displacement of the original points a distance h_e in the direction normal to the surface.

Following these steps, a new airfoil geometry is obtained that is employed by construct2D to generate the computational grid. Nevertheless, Figure 25 shows one of the preliminaries meshes that were obtained with the tool. As can be seen, the desired surface of the airfoil is not obtained because construct2D was configured to redefine the points of the airfoil geometry. Two main problems were detected and needed to be solved. First, the eroded geometry of the airfoil must be respected in order to adequately model the phenomena of erosion. To do it, the construct2D settings were modified to respect the geometry. Therefore, each given geometry point would represent a vertex of the mesh. Secondly, low quality meshes were obtained at the transitions between the original and the eroded surfaces of the airfoil. Construct2D lacks the capability to define refinement regions and struggles to obtain good meshes at the steps produced by the erosion.

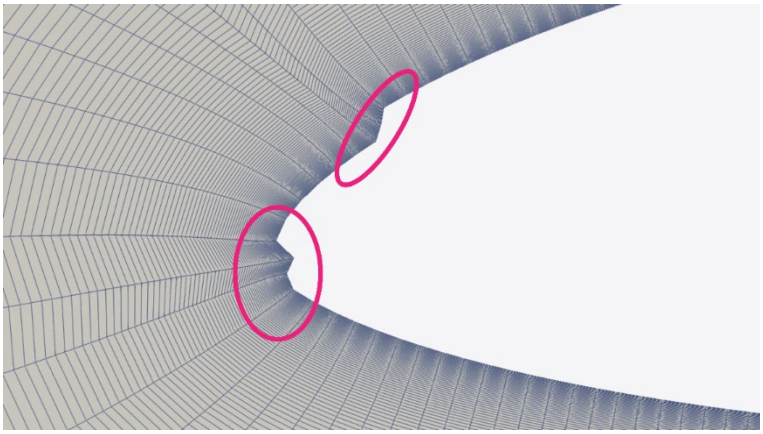

Figure 25 Wrongly eroded geometry of a DU95W180 airfoil. The worst areas are surrounded by pink circles. This first attempt of geometry modification was unsuccessful.

Two options were considered to address this issue. Employing a structured grid generator or modify the eroded-to-clean transition. Table 5, collects the main advantages and disadvantages of the two approaches considered.

Table 5 Advantages and disadvantages of the two approaches considered to obtain the computational grid to model erosion

Option	Advantages	Disadvantages
Structured grid generator, ICEM	• Better resolution of the erosion steps • High capacity to define the grid topology and characteristics	• Grid generation difficult to automate • Higher mesh non orthogonality • Quality depends on the user's experience
Modification of the eroded-to-clean transition	• Easy to automate • Low resolution of the flow close to the steps	• Does not represent the most detrimental damage • Mesh quality needs to be checked

The objective of the tool is to analyse different airfoil geometries in order for the APM tool to extrapolate the estimations to airfoils not considered during the training model. Therefore, it is required to employ a fast and reliable tool to be included in a highly automatable workflow. On the EOLIA project report (Saenz, Méndez-López, & Muñoz, 2022), several patterns of erosions were studied and was found that defining a 45-degree slope on the eroded-to-clean transition was the second more harmful pattern. It must be taken into account that the actual erosion pattern is not known, and that this approximation is usually found in literature. Figure 26 shows the final erosion pattern that was considered in the simulations.

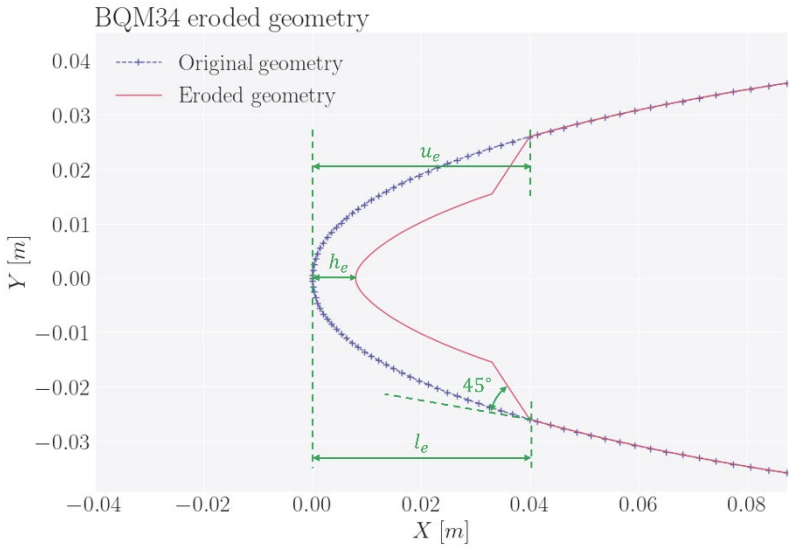

Figure 26. The final erosion pattern is obtained applying a 45° slope. On blue, the original geometry of an BQM34 airfoil is presented. The final eroded geometry, that will be simulated, is coloured in pink.

This modification of geometry has been tested on the DU95W180 airfoil. Three erosion depths have been considered as well as 2 different erosion extension. At the Table 6 the 11 simulations considered are described. The objective of the comparison is to evaluate in terms of aerodynamic performance the influence of the leading-edge erosion. Cases 1 and 2 represent values of erosion between categories c and d of Figure 12, cases 4 and 5 are close to category d and cases 5 to 8 present an erosion of category e.

Table 6 Description of the simulations performed with the airfoil DU95W180

Case name	Re (millions)	h_e	l_e	u_e
Case 1 clean	6	0	0	0
Case 2 clean	9	0	0	0
Case 3 clean	12	0	0	0
Case 1	6	0.001	0.01	0.01
Case 2	6	0.001	0.04	0.04
Case 3	6	0.004	0.01	0.01
Case 4	6	0.004	0.04	0.04
Case 5	6	0.008	0.01	0.01
Case 6	6	0.008	0.04	0.04
Case 7	9	0.008	0.04	0.04
Case 8	12	0.008	0.04	0.04

Figure 27 presents the lift curves obtained for cases 1 to 6 compared to the corresponding clean condition (case 1 clean). For each erosion depth, two extensions have been considered. The lower extensions ($u_r = l_r = 0.01$) are depicted on dots while the higher erosion ($u_e = l_e = 0.04$) are shown with squares. The red colour is employed on the softer erosion ($h_e = 0.001$), green colour for mild erosion ($h_e = 0.004$) and hard erosion ($h_e = 0.008$) is shown in yellow. The blue line represents the clean condition of the airfoil. It must be noted that case 3 and 5 have not converged at all angles of attack. Some angles of attack are discarded due to convergence criteria, those higher than 10 and 8 degrees for cases 3 and 5 respectively.

At angles lower than 3 the influence of the considered erosions is negligible on the lift coefficient. However, differences arise at higher angles of attack and close to the stall region. Table 1 presents the parameters most influenced by the erosion. It can be seen that the maximum lift is reduced up to a 34.4% from the clean condition on case 6. This reduction, together with the increase of the drag coefficient provoke the reduction of the efficiency. Again, case 6 is the most affected by the erosion resulting in a 43.6% decrease of the efficiency. The erosion also provokes a shift on the angle of attack at where the maximum efficiency is obtained as shown in Figure 28.

Table 7 Influence of the erosion on maximum lift, stall angle, maximum efficiency and the angle at which occurs.

Case	Clean 1 (reference)	Case 1	Case 2	Case 3	Case 4	Case 5	Case 6
Maximum lift	1.187	-15.6 %	-11.2 %	-27.9 %	-27.7 %	-29.2 %	-34.4 %
AoA of stall	10	9	9	7	8	8	8
Maximum efficiency	78.06	-14.5 %	-13.2 %	-24.7 %	-30.9 %	-29.9 %	-43.6 %
AoA of max. efficiency	7	6	6	4	4	4	4

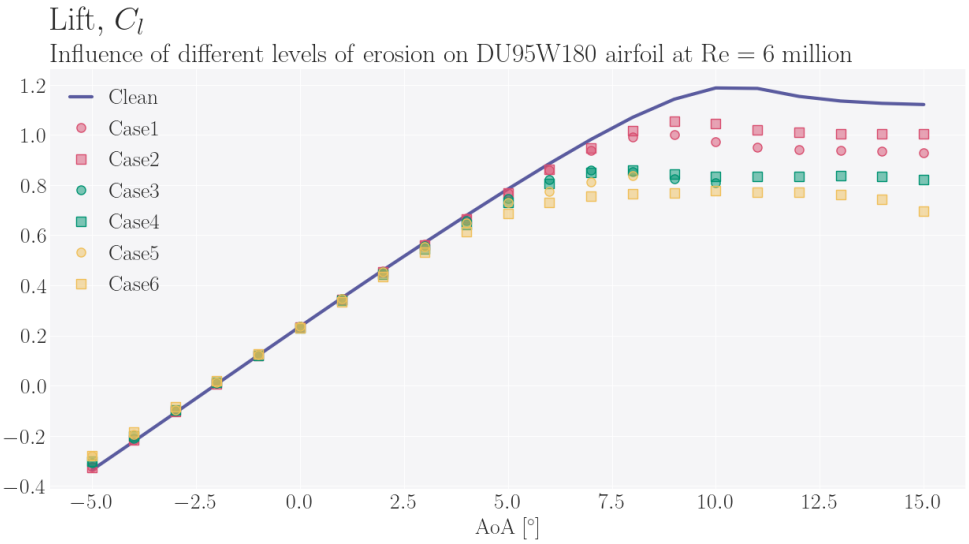

Figure 27 Comparison of the lift curves at Reynolds 6 million with different levels of erosion.

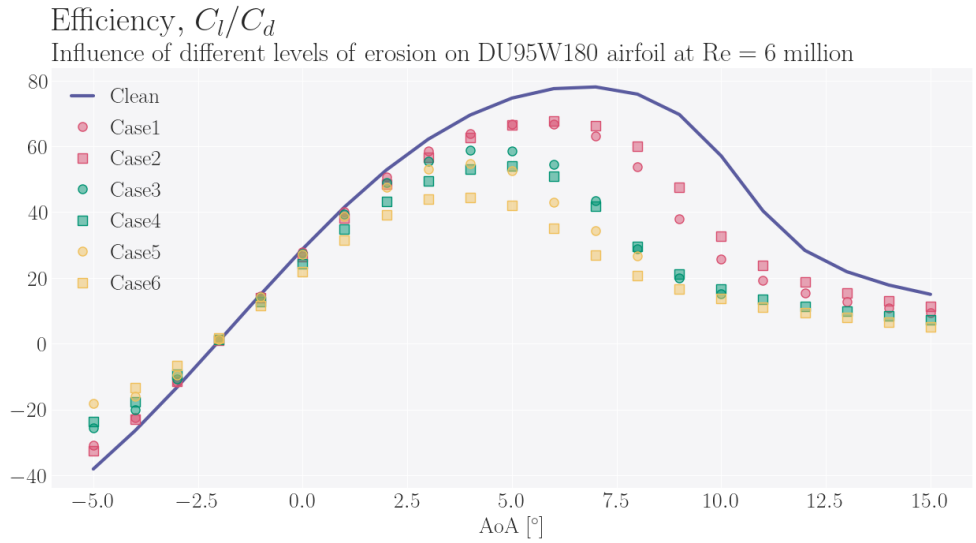

Figure 28 Comparison of the efficiency curves at Reynolds 6 million with different levels of erosion.

From the previous results it can be concluded that increasing the height of the erosion induces a reduction of the lift and efficiency while reduces the angle of attack at which the stall and maximum efficiency occur. The influence of the affected length increases the loss of performance with $h_e = 0.004$ and $h_e = 0.008$. This is not the case with the lower erosion severity, $h_e = 0.001$.

In addition, for the most severe case $h_e = 0.008, l_e = u_e = 0.04$ the influence of the Reynolds number is also analysed. Figure 29 shows the comparison of these cases (clean 1, clean 2, clean 3, clean 6, clean 7 and clean 8 from Table 6). The results of the clean cases are presented using solid lines, while the points represent the eroded ones. The blue, red and green colours correspond to Reynolds of 6, 9 and 12 million respectively. At the three Reynolds numbers the erosion provokes a reduction of lift and efficiency as well as an increase on drag, as expected. Nevertheless, while the degradation of the aerodynamic performance is greater at higher Reynolds numbers, the variation of the Reynolds number on the eroded cases has almost none influence at the three coefficients. Differences arise at higher angles of attack, presenting higher values of lift and drag coefficients while Reynolds increases. Even though, the resulting efficiency curves present negligible efficiency. The maximum values of efficiencies are 44.45, 44.48 and 46.2 for eroded cases at Reynolds 6, 9 and 12 respectively.

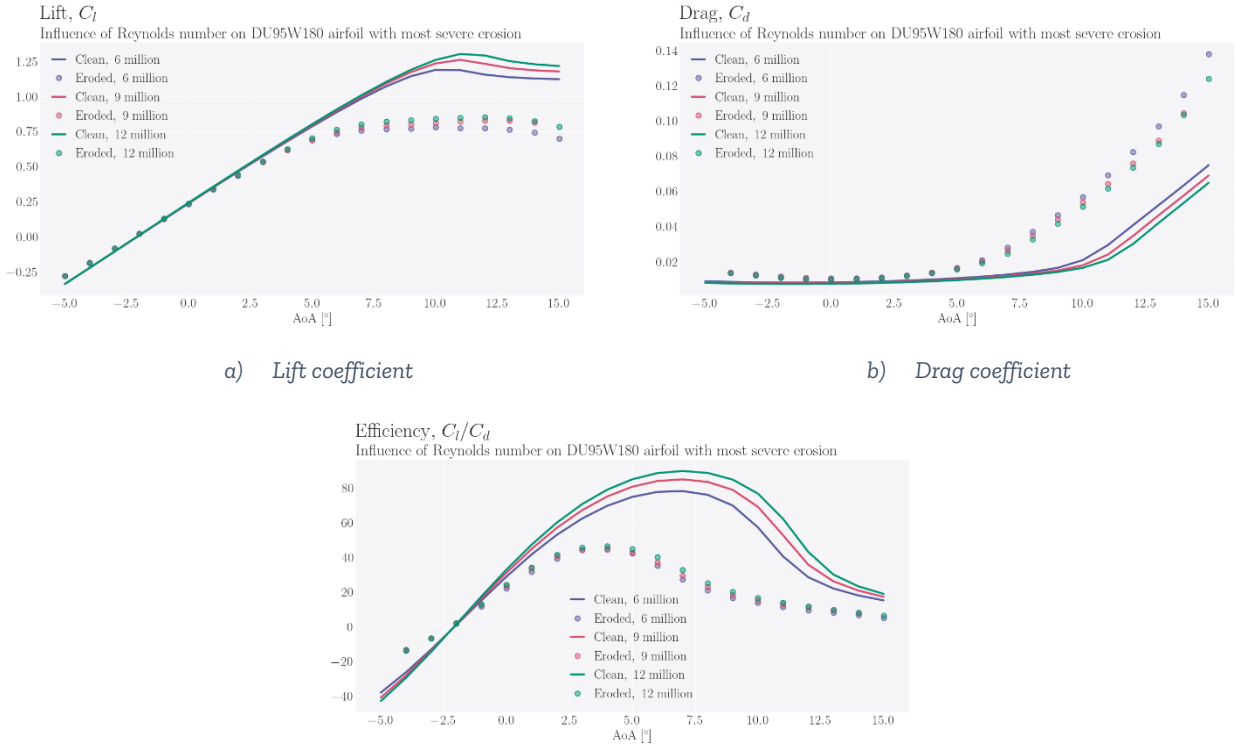

a) *Lift coefficient*

b) *Drag coefficient*

c) *Efficiency*

Figure 29 Comparison of the lift (a), drag (b) and efficiency (c) coefficients of the DU95W180. The clean and class e eroded curves are compared at Reynolds numbers of 6, 9 and 12 million.

From the blade inspections available, roughness and erosion appeared on the outermost 25% of the wind turbine blades. Actual chord distribution of the inspected blades was not available. Therefore, the NREL 5MW (Jonkman, Butterfield, Musial, & Scott, 209) was employed to determine the Reynolds number distribution over the blade span. At Figure 30 the Reynolds number distribution is shown. The airfoils considered on this blade belong to DU and NACA families. As can be seen the Reynolds numbers ranges from 3 to 8.5 million. The half outer part of the blade present Reynolds number higher than 5 million. Therefore, the selected Reynolds number (6, 9 and 12 million) on the previous comparison is significant as they represent the Reynolds of modern wind turbines in the sections most prone to erosion.

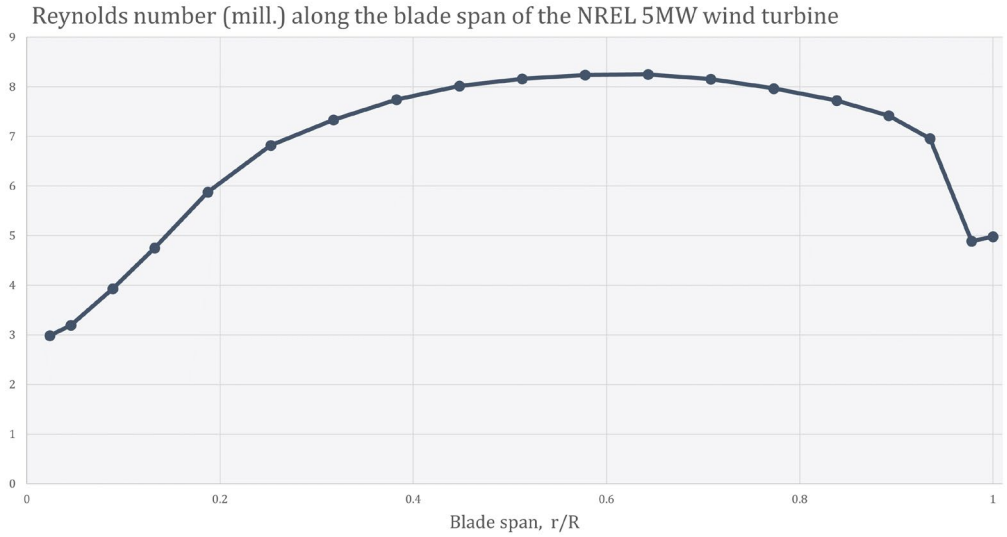

Figure 30 Reynolds number distribution over the blade span of the NREL 5MW research wind turbine.

4 Model summary and tool development (airFoam)

This section summarizes all the modelling decisions made to generate the aerodynamic dataset to be employed on the tool development.

Table 8 Objectives and decisions made

Objective	Decision
APM tool aims to estimated accurately airfoils not considered in training	Variety of airfoil shapes will be considered: • Construct2D tool to generate computational grids • A slope of 45 degrees is considered at the erosion-to-clean transition
Reduced computational cost	Roughness considered with Cebeci model Wall functions will be employed Fully turbulent approach on all simulations
Modern wind turbines	Reynolds numbers from 6 to 12 million
Erosion and roughness with significant influence	Located at the 25% outermost part of the blade Airfoil thickness considered from 10% to 30%

The following ranges of roughness and erosion have been determined to be analysed from blade status categories of SALT tool and IEA Task 46. Table 9 collects the parameter values considered during the dataset generation. In addition, clean simulations are also performed at the specified Reynolds numbers. This results in 3465 simulations, each one corresponding to one angle of attack, for each airfoil considered.

Table 9 Values of blade status parameters considered

Parameter	Values
Roughness height, h_r	$1 \times 10^{-5}, 2.5 \times 10^{-5}, 5 \times 10^{-5}$
Upper side rough length, u_r (chord percentage)	$10, 15, 20$
Lower side rough length, l_r (chord percentage)	$10, 15, 20$
Erosion height, h_e (chord percentage)	$0.1, 0.4, 0.8$
Upper side eroded length, u_e (chord percentage)	$1, 2, 4$
Lower side eroded length, l_e (chord percentage)	$1, 2, 4$
Reynolds number, Re (millions)	$6, 9, 12$
Angles of attack (min, max, step)	$-5, 15, 1$

The huge number of simulations required to generate the dataset encourages the development of an automated workflow that has been called airFoam. Figure 31 shows the steps implemented in airFoam. As inputs, this tool needs the definition of the airfoil coordinates, in XFoil format and counterclockwise ordering, and the simulation parameters. The simulation parameters employed are those described in Table 9, other values could be defined by the user if necessary.

Figure 31 Airfoam workflow

With these inputs, all the considered angle of attack simulations are prepared. All the simulations for the same airfoil and Reynolds number employ the same computational grid. For the rough cases, the airfoil surface is divided into 2 regions corresponding to the rough and clean regions of the surface. For the eroded cases, only the leading edge of the airfoil is modified according to the erosion parameters. Therefore, the difference between the eroded and other meshes is due to the geometry modification performed to consider the leading-edge erosion. These grids are generated by construct2D tool which its employment delivered satisfactory results compared to wind tunnel measurements described in Section 2 and demonstrated its ability to model erosion on Section 3.3. All computational grids are checked thoroughly and those that do not comply with quality standards are not considered.

Once the simulation setups are prepared, each AoA simulation is submitted automatically on the CENER HPC cluster. Simulations are run for a maximum of 10,000 iterations and convergence is controlled by the monitoring of the residuals. The convergence criteria are set to 1e-7 for all variables. Nevertheless, close to the stall region and on eroded cases, the convergence criteria are relaxed. To consider a simulation converged it has been required that any of the three aerodynamic coefficients must have a standard deviation over the last 4,000 iterations lower than a 5% of the mean value.

AirFoam post-processes the results automatically once all the angles of attack have been simulated obtaining:

- Lift, drag and moment coefficients (c_l, c_d, c_m)
- Pressure coefficient distribution over the upper and lower sides (c_p)
- Wall shear stress distribution over the upper and lower sides

Moreover, flow field variables are also saved in VTP format. The airFoam tool development has represented a significant milestone within the task 3.3 as it:

- Automates the grid generation.
- Automates the definition of rough areas.
- Automates the modification of the airfoil geometry due to erosion.
- Automates the generation of the simulation setups eliminating any configuration errors and ensuring that each angle of attack is computed with the same grid and numerical schemes.
- Eases the dataset generation by providing one file per airfoil containing all the required aerodynamic information.

Regarding the numerical schemes, convective terms are discretized using a second-order upwind schemes, balancing between accuracy and numerical stability. The convection of turbulent variable was discretized with a first order accuracy upwind scheme. For the diffusive terms, a corrected central differencing scheme was employed which corrects for mesh non-orthogonality. Gradient terms were computed using also a central differencing scheme which is second order accurate. Pressure-velocity coupling was handled using the SIMPLE algorithm. These choices ensure stable and reliable simulations with a balance between computational cost and solution fidelity.

5 Airfoil performance model

By means of machine learning algorithms, the Airfoil Performance Model will estimate the aerodynamic performance of an airfoil considering it surface status. The tool should cover the following features

- Applicability to wind turbines blades, covering airfoils located at the 25% outermost part of the blades. This limits the range of thickness and Reynolds numbers at which the wind turbine will give accurate results.
- Accurate prediction of the aerodynamic performance of an airfoil considered in the training dataset.
- General use, the tool should be able to extrapolate to new airfoils not considered within the training dataset. A range of usability will be given.

As the tool is intended to estimate the aerodynamic performance of airfoils not considered during the training a variety of airfoil shapes has been selected with thickness ranging from 7.5% to 30%.

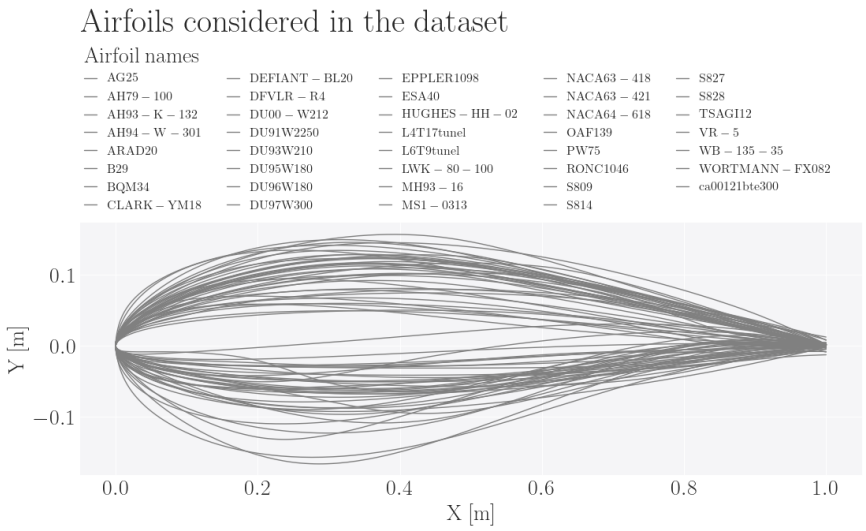

Figure 32 Airfoil geometries and airfoil names employed to generate the dataset

5.1 Geometry parametrization and airfoils description

The geometry of an airfoil can be defined in several ways. The most common is defining a certain quantity of points known as geometry coordinates. The number of points may depend on the airfoil complexity. ML algorithms usually require a uniform description of the features of the dataset, so the number of points employed to define all the airfoils considered should be the same. Based on its experience, CENER usually employs 345 points to describe the airfoil geometry. Nevertheless, this results in too many geometric parameters. A common rule of thumb is to have at least 10 times as many samples as the number of features. Therefore, to reduce the geometrical features it is needed parametrize the geometry.

Two approaches have been considered:

- Bezier parametrization: the camber and thickness curves are obtained from the airfoil geometry, and each is fitted with a 5^{th} degree Bezier curve. The geometrical parameters are the control points of those fitted curves.
- PARSEC parametrization: the parameters employed in this parametrization are physically related to the airfoil geometry, e.g. radius at the trailing edge, upper surface maximum thickness.

Below, a more thorough description of these two parametrizations is given. Two models will be trained, one per each parametrization, and the results will be compared to determine which one yields more accurate estimations.

5.1.1 PARSEC parametrization

The PARSEC parametrization is a method used for defining airfoil shapes through a set of parameters that describe the geometry of an airfoil in a compact and efficient way. This parametrization is particularly useful in optimization and design task. The PARSEC parametrization involves the following set of parameters:

- Leading Edge Curvature Radius, r_{le}.
- Upper surface at maximum thickness given by its coordinates, x_{mu} and y_{mu}.
- Upper surface curvature at maximum thickness, k_{mu}.
- Lower surface at maximum thickness given by its coordinates, x_{ml} and y_{ml}.
- Lower surface curvature at maximum thickness, k_{ml}.
- Trailing edge direction, α_{te}.
- Trailing edge wedge angle, β_{te}.
- Trailing edge vertical location, z_{te}, and its thickness, Δ_{te}

The main advantage of this parametrization is that it directly controls important geometric features which eases the understanding of how aerodynamic performance is affected by geometric modifications. It results in 11 features allowing to reduce the number of computations required. This compact representation might not be able to represent all possible airfoil shapes, especially those unconventional. In fact, it was found that retrieving the original geometry from the PARSEC parameters was challenging and with poor results.

Table 10 shows the statistical distribution of the values obtained for each one of the 39 airfoils with the PARSEC parametrization.

Table 10 Statistical distribution of the PARSEC parametrization for the 39 considered airfoil.

Metric	l_{re}	x_{mu}	y_{mu}	κ_{mu}	x_{ml}	y_{ml}	κ_{ml}	α_{te}	β_{te}	z_{te}	Δ_{te}
Mean	0.01855	0.354259	0.105704	0.956216	0.31039	-0.06903	1.043305	11.90897	9.035172	0	0.004904
Std.	0.015415	0.066168	0.02945	0.387047	0.093328	0.035543	0.879916	7.727254	10.90125	0	0.004681
Min.	0.004043	0.190587	0.049501	0.296375	0.035006	-0.16598	0.153536	0.858234	0.110994	0	0.0008
25%	0.008077	0.321594	0.080193	0.657952	0.264918	-0.08859	0.411523	6.259487	2.695309	0	0.003269
50%	0.012351	0.352891	0.112482	0.960589	0.317397	-0.06273	0.735624	11.4835	5.324564	0	0.0033
75%	0.026771	0.390878	0.126477	1.259715	0.358267	-0.04707	1.543597	15.81963	11.39523	0	0.003566
Max.	0.081736	0.493382	0.156849	1.670507	0.509158	-0.01163	3.969904	30.64185	60.33523	0	0.024996

5.1.2 Bezier parametrization

As stated, the approach to parametrize the geometry employing a Bezier curve fitting is based on the control points that define the fitted curves. CENER employs this parametrization in its own airfoil-design tool (airfoilDT) and therefore it was the first parametrization to be considered. The workflow is summarized below:

1. Based on an XFoil coordinate file, the number of points that define the geometry is set to 345. XFoil is employed to do so. The airfoil is also normalized to have a 1 m chord and the chord aligned with the X axis.
2. Camber and thickness curves are obtained following the British convention in which the thickness is measured perpendicular to the airfoil chord line.
3. Camber and thickness curves are fitted to a n-th degree Bezier curve, represented by n+1 control points. The residual of the fitting is defined as the RMSE between all the fitted points and the originals. The fitting process is finished when the residual value is lower than 1e-6 or a maximum

of 10000 iterations is reached. The following restrictions are considered:

   a. First and last control points of each curve are coincident with the initial and final points of the original curve.
   b. To ensure a smooth trailing edge, the second control point is forced to be on the vertical direction of the first one.

4. Each one of the control points are defined by its longitudinal and vertical positions.

The main reason to consider this parametrization is that a similar parametrization is implemented in CENER's arifoilDT. This would facilitate the coupling between both tools allowing to employ the APM as the aerodynamic module responsible for the performance evaluation.

To determine the appropriate degree of the Bezier curves, a comparison between two approaches has been made. The first one employs a 3rd degree fitting of the camber curve and a 4th degree of the thickness one. The other employs a 5th degree fitting of both curves. Both approaches were compared with NACA63-418 and CA00121 airfoils.

Figure 33 shows the parametrization of the camber (upper figure) and thickness (lower figure) for the NACA63-418 airfoil. This airfoil has simple camber and thickness curves with no inflexion points and no abrupt changes of curvature. The results from the first approach are depicted on pink, using a 3rd degree Bezier curve for camber and 4th for thickness. On green, the results from second approaches using a 5th degree curve for both curves are plotted on green. Solid blue line represents the original curves and solid pink, and green lines represent the fitted curve with approaches 1 and 2 respectively. The dotted lines with circles represent the control points of the respective Bezier curves. Because the simplicity of the original curves, both approaches result in a satisfactory fit of the original curve. This is not the case of CA00121 airfoil.

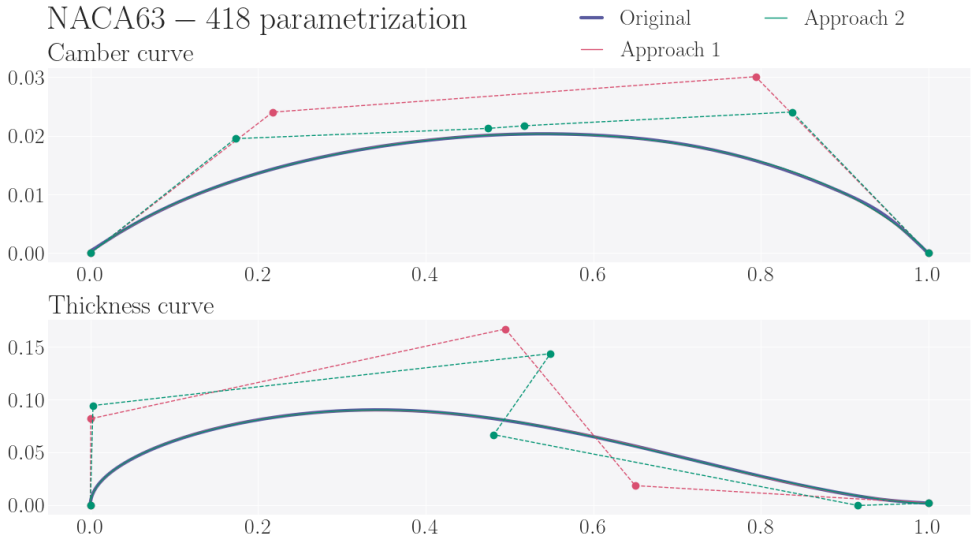

Figure 33 Parametrization of the NACA63-418 airfoil with Bezier curves. Two approaches are compared, approach 1 employs 4 control points while approach 2 employs 6.

The CA00121 airfoil was designed by CENER aiming to obtain an increased efficiency with no abrupt decrease of the efficiency close to the design angle of attack. This resulted in more complex camber and thickness curves with changes of curvature of the curves. Figure 34 compares the resulting parametrizations. Lines are depicted as in Figure 33. While both approaches are able to represent adequately the thickness curve, a 4th degree curve is able to represent the two inflection points, the approach 1 catastrophically fails to represent the camber curve. As can be seen in the upper plot of Figure 34, the obtained second and third control points result in a miss-representation of the camber curve.

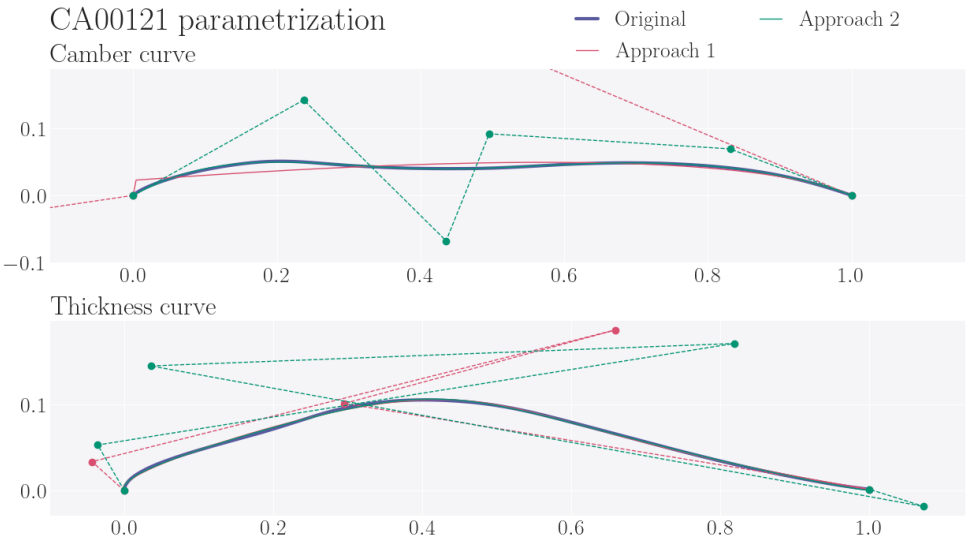

Figure 34. Parametrization of CA00121 airfoil with Bezier curves. Two approaches are compared, approach 1 employs 4 control points while approach 2 employs 6.

It is true that the CA00121 is the oddest airfoil shape considered, but a proper parametrization needs to be employed. Therefore, a parametrization employing 5^{th} degree curves is selected to generate the dataset as it does not increase significantly the number of geometric features while it ensures an adequate representation of the airfoil. The following naming convention is followed: longitudinal position of the control points is represented by x, vertical position with y, control points of the camber curve are followed by a c while those of thickness curve use a t, finally the number of the control point is used starting by 0. This parametrization may also be referred as *xiyi* in some parts of the deliverable. It must be noted that even though 12 control points are employed, 6 per curve, only 16 geometric features are considered as initial and final point as the following positions are restricted:

- Longitudinal and vertical position of the initial and final point of the camber curve $(xc0, yc0, xc5, yc5)$.
- Longitudinal and vertical position of the initial point of the thickness curve $(xt0, yt0)$.
- Longitudinal position of the second point of the thickness curve $(xt1)$.
- Longitudinal position of the final point of the thickness curve $(xt5)$.

The statistical distribution of the geometric features obtained with the aforementioned parametrization are shown in Table 11 (camber curve control points) and Table 12 (thickness curve control points). These two tables are obtained from the 39 airfoils that will form the dataset employed to train and validate the model.

Table 11 Statistical distribution of the camber curve parameters.

Metric	$xc1$	$xc2$	$xc3$	$xc4$	$yc1$	$yc2$	$yc3$	$yc4$
Mean	0.09366301	0.485085236	0.506834891	0.811636959	0.02466788	0.01671462	0.025353991	0.021650957
Std.	0.338179761	0.270765219	0.178852012	0.060054953	0.035810896	0.032737021	0.035413256	0.027023938
Min.	-1.8226555	-0.5574578	-0.3438232	0.6349185	-0.0495966	-0.0687620	-0.0743321	-0.0355078
25%	0.097085776	0.39844241	0.449245959	0.789739625	0.002640423	2.04E-05	0.003346961	0.002683115
50%	0.170642396	0.488926259	0.512978852	0.828423657	0.026849979	0.020827063	0.026245969	0.021871998
75%	0.199991202	0.583750956	0.599975008	0.850684801	0.044391237	0.036369995	0.046993299	0.043706334
Max.	0.334835074	1.54257469	0.800077312	0.915637642	0.142360384	0.092440812	0.093019079	0.071035449

Table 12 Statistical distribution of the thickness curve parameters.

Metric	$xt2$	$xt3$	$xt4$	$yt1$	$yt2$	$yt3$	$yt4$	$yt5$
Mean	0.542323649	0.471889678	0.907928326	0.084971867	0.143074702	0.055031985	0.010557627	0.002442231
Std.	0.156940566	0.222696161	0.13183462	0.03214822	0.078658714	0.038563683	0.021087952	0.002344071
Min.	0.121151263	-0.05980454	0.559357147	0.014258724	0.011628282	-0.0323634	-0.0208142	0.0004
25%	0.443052764	0.331409869	0.878327989	0.06435323	0.07883059	0.037475811	5.11E-05	0.0016225
50%	0.540791521	0.465287232	0.904173884	0.083446089	0.140779804	0.056583825	0.006104913	0.001643
75%	0.644302351	0.580919955	0.957928736	0.099393061	0.183729876	0.073424815	0.016162027	0.001783
Max.	0.810267327	1.016183012	1.273136407	0.204382152	0.332699897	0.162152364	0.095775094	0.012498

This distribution is better shown on Figure 32 where a boxplot is employed. Green line represents the median value of the parameters while the box upper and lower limit represent the Q3 and Q1 values. The whiskers extend from the edges of box to show the range of the data, but they extend no more than $1.5 \times (Q3 - Q1)$. Values outside from this range are considered outliers and plotted as separate dots. It is believed that any airfoil whose geometric features lay inside the whiskers may be properly estimated but this hypothesis needs to be confirmed.

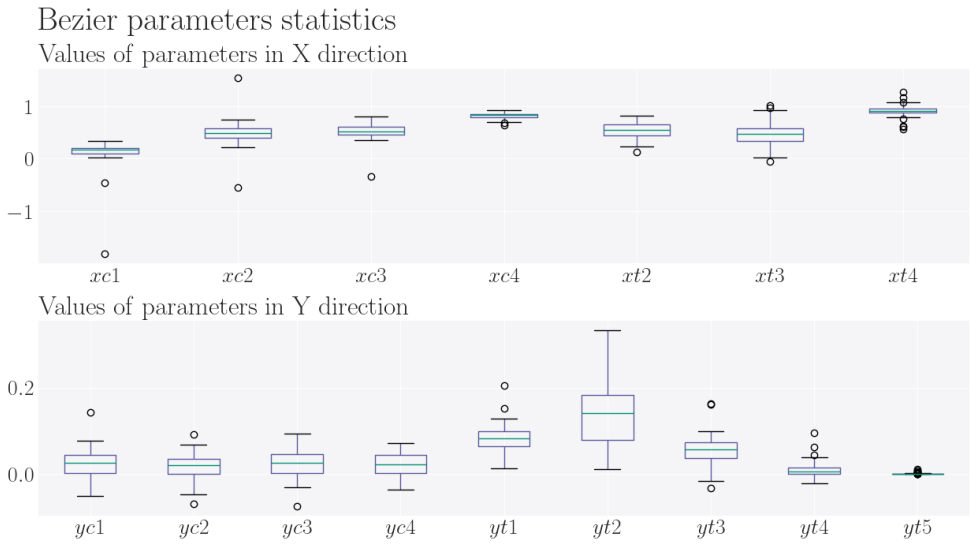

Figure 35 Statistical distribution of the Bezier parametrization. The geometric dataset is composed by the 39 airfoils shown in Figure 32.

5.2 Surface status parametrization

On sections 2.2 and 3.3 the parametrization of the rough and erosion status has been explained. On figures Figure 8 and Figure 26 a visualization of the parameters is presented. The values of the parameters that have been employed to generate the dataset are shown in Table 9.

5.3 Dataset generation and analysis

To create the dataset the tool airFoam, described in Section 4, has been employed with the parameters from Table 9. The airfoils that have been simulated are those depicted on Figure 32. The combination of the parameters detailed in Table 9 results in 63 angles of attack under clean conditions and 1701 under erosion and roughness. A total of 3465 simulations per airfoil considered are simulated. Figure 36, Figure 37 and Figure 38 present the percentage of converged simulations per airfoil. The maximum value of the horizontal axis is 100 meaning that all the simulations have converged. The percentage on Figure 36 is grouped by the Reynolds number, while Figure 37 is grouped by the surface status and Figure 38 by the range of angle of attack. The percentage is computed within each group, e.g., the clean simulations

on Figure 37 have a maximum value of 33% meaning that all clean simulations are converged even though only 63 clean simulations are computed by airfoil.

It can be seen on Figure 26 that the airfoils with lower convergence are: AG25, BQM34, LWK-80-100, OAF139 and WORTMANN-FX082. These five airfoils have a thickness lower than 14%. The average percentage of convergence per Reynolds are 29.75%, 30.2% and 30.8 % for Reynolds 6, 9 and 12 million. A similar rate of convergence is obtained for all three Reynolds numbers.

As stated in Section 3.3, the computational grids of the eroded conditions are complex to obtain. Therefore, a thorough quality verification of the grids is made. Airfoils AH94-W-301, ARAD20, BQM34, LWK-80-100, PW75 and S828 present a geometry that did not allowed to model the erosion adequately and therefore this condition was not simulated resulting in a zero-convergence percentage on Figure 37. A 32.2% (maximum is 33.33%) of the clean simulations are converged while only a 25% of the eroded ones achieved convergence. This behaviour was expected as the flow becomes more complex and unsteady. The convergence of roughness simulations is 31%. This means that a 96.6 %, a 93% and a 75% of the angles of attack are converged of the clean, rough and eroded conditions.

The simulated angles of attack have been grouped in 4 ranges with a step size of 5 degrees. It must be noted that this results in a maximum value of convergence per range of 25%. As expected, higher angles of attack which are closer to or into the stall region present the lower rate of convergence, 18%. Again, the lower convergence is achieved on airfoils AG25, BQM34, LWK-80-100, OAF139 and WORTMANN-FX082. Their convergence at higher angles of attack is lower of 2.5%. The other three ranges present adequate convergence rates of 23.8 %, 24.8% and 23.6%.

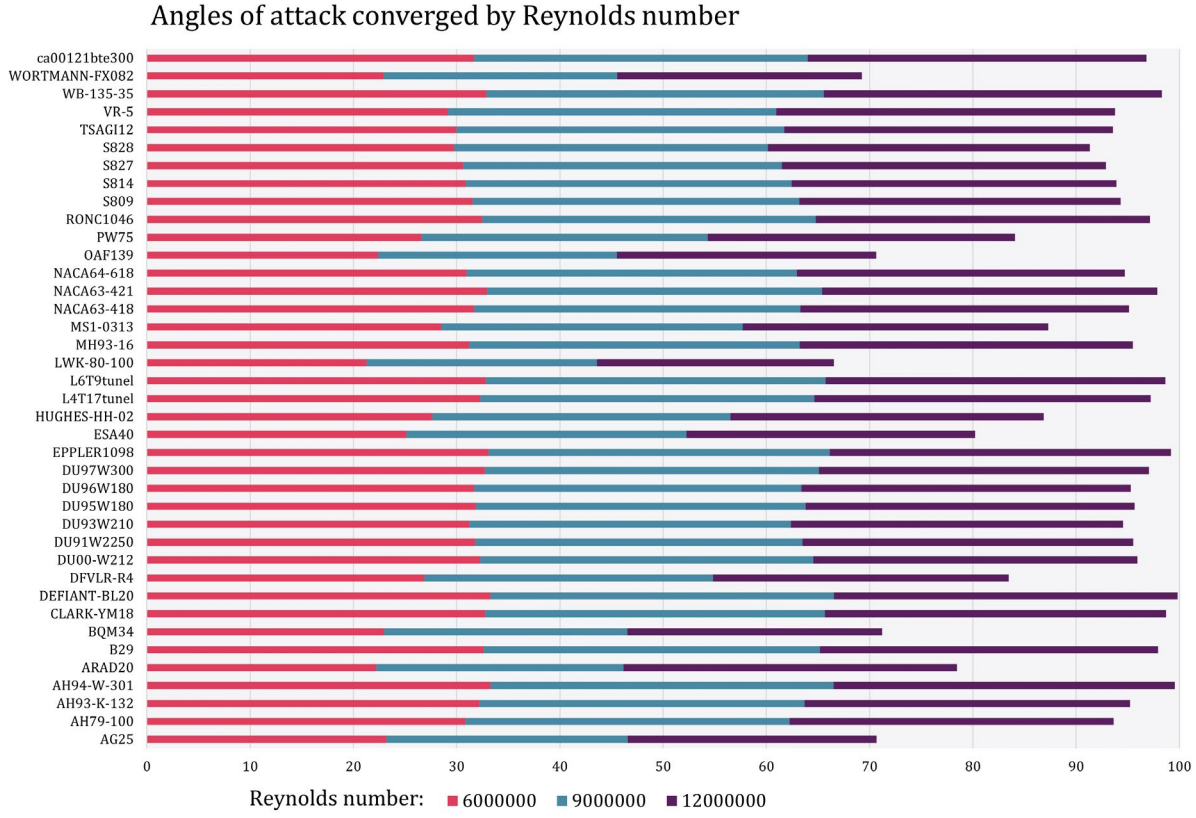

Figure 36 Percentage of converged simulations grouped by Reynolds number.

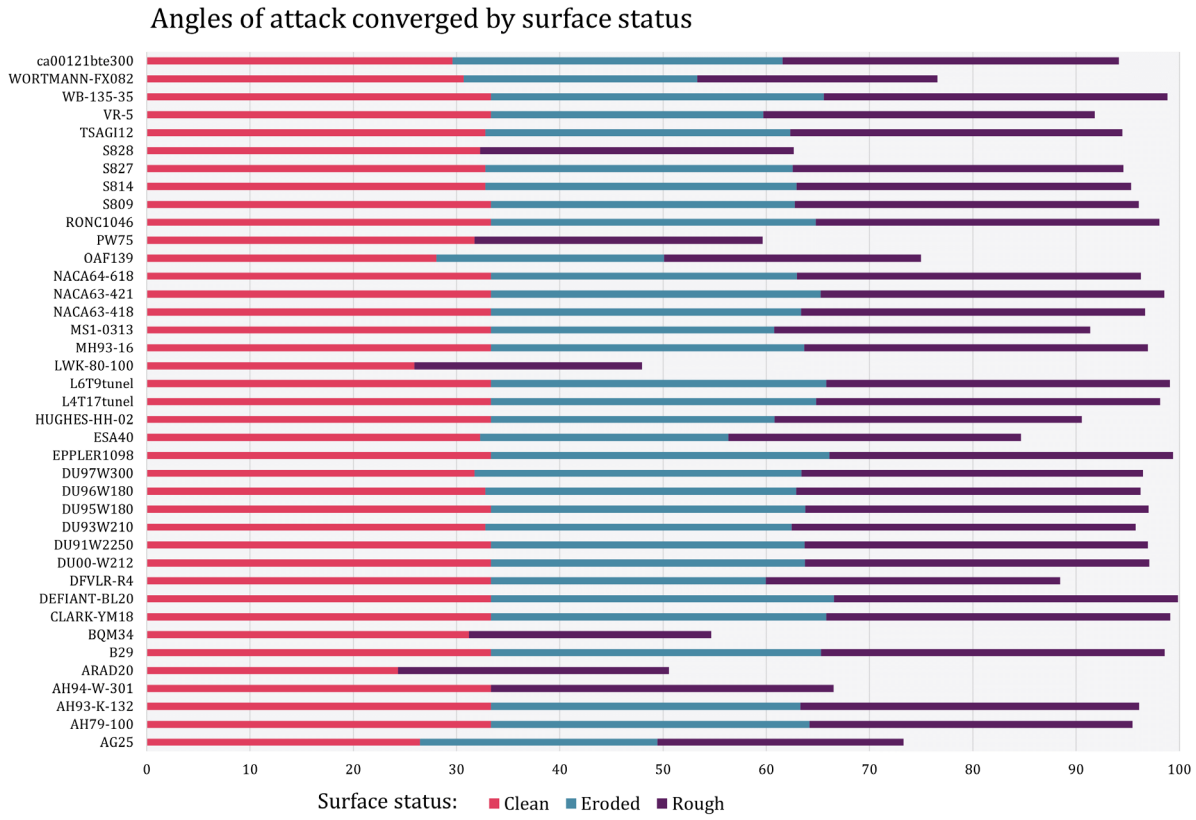

Figure 37 Percentage of converged simulations grouped by surface status.

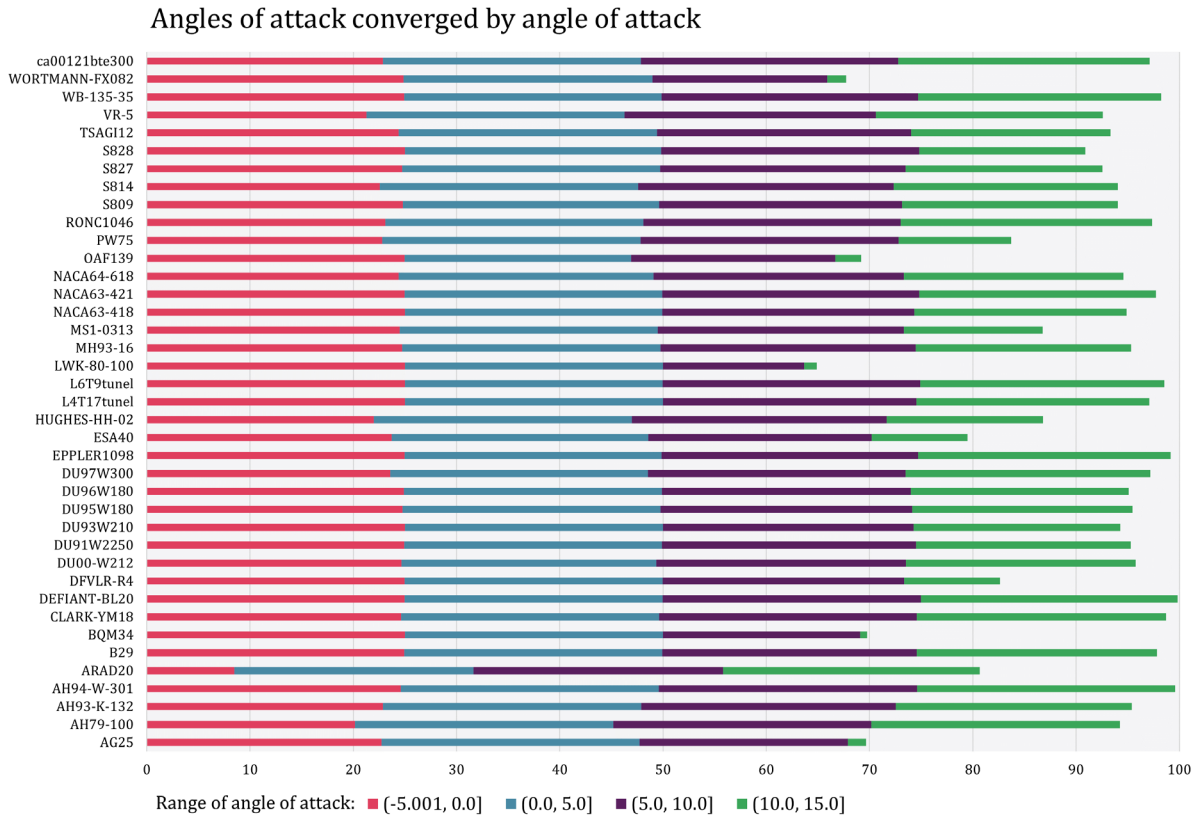

Figure 38 Percentage of converged simulations grouped by range of angle of attack.

On Figures Figure 39, Figure 40 and Figure 41 the statistical distribution of lift and drag coefficients obtained are presented. Figure 39 presents the values at Reynolds number of 6 million, Figure 40 at 9 million and Figure 41 at 12 million. The boxplots have the same configuration than those on Figure 35. All three conditions, i.e. clean, rough and eroded, are considered on the plots. At higher angles of attack there is more deviation on the values of drag coefficient. These plots, together with Figure 35, allow to analyse why an airfoil is properly predicted or not. If an airfoil with and aerodynamic behaviour out of the distribution is estimated it is expected to not be accurate. Nevertheless, it is more important to define the range of application of the APM only with the geometric features as those are employed as an input and the aerodynamic coefficients are presumably not known. As the roughness and eroded conditions represent most of the angles of attack simulated and they produce a deterioration of the aerodynamic performance the clean conditions will always show higher values of lift and are considered as outliers.

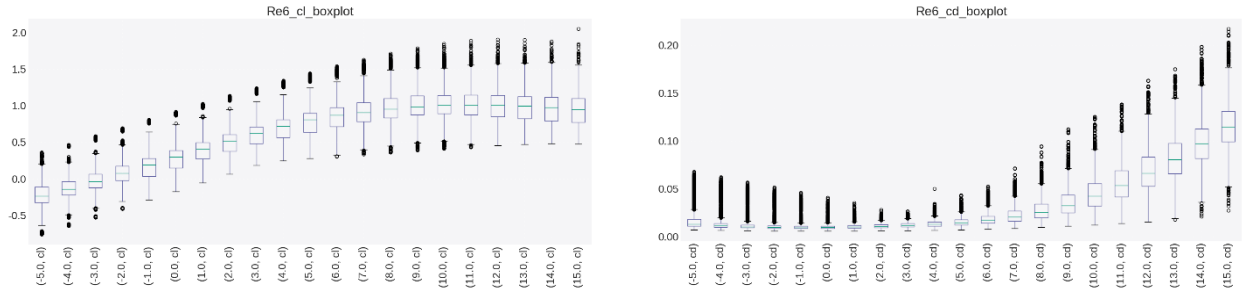

c) *Lift coefficient* d) *Drag coefficient*

Figure 39 Statistical analysis of the dataset generated. Lift (a) and drag (b) coefficients at Reynolds 6 million.

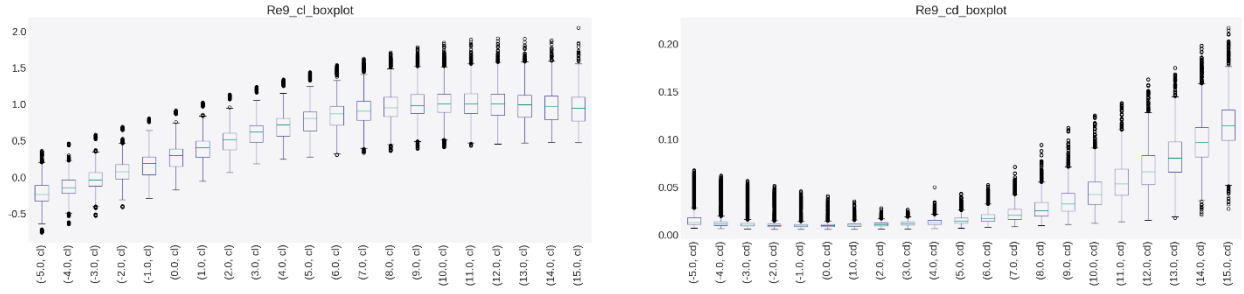

a) *Lift coefficient* b) *Drag coefficient*

Figure 40 Statistical analysis of the dataset generated. Lift (a) and drag (b) coefficients at Reynolds 9 million.

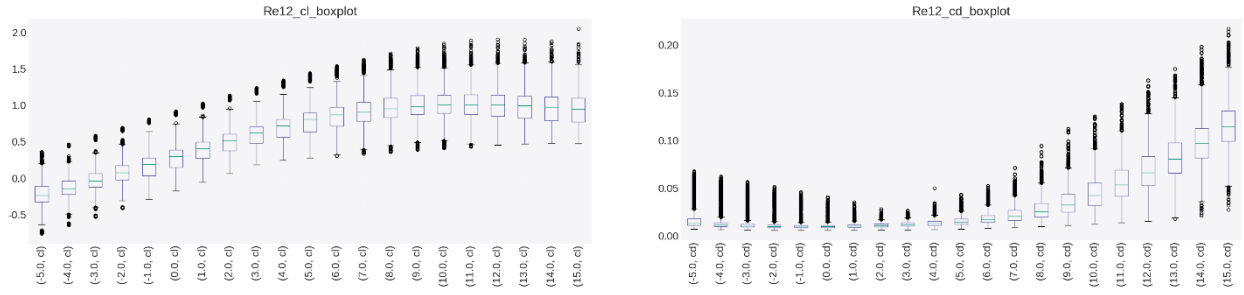

a) *Lift coefficient* b) *Drag coefficient*

Figure 41 Statistical analysis of the dataset generated. Lift (a) and drag (b) coefficients at Reynolds 12 million.

The dataset that has been generated can be employed to further understand the influence of the airfoil geometry on its aerodynamic performance under rough and eroded conditions.

5.4 Algorithm comparison: Random forest vs Neural Networks

In the field of aerodynamics, accurate estimation of the aerodynamic coefficients, i.e. lift, drag and efficiency, is crucial for the optimization and design of airfoils. As explained, these coefficients are highly influenced by the airfoil geometry, angle of attack, Reynolds number or surface status. Computational Fluid Dynamics (CFD) simulations provide detailed insights of the aerodynamic performance, yet they are computationally intensive. Moreover, the modelling of roughness or erosion on the leading edge of the airfoil requires extensive experience in aerodynamics and CFD. Therefore, the development of surrogate models based on machine learning techniques can offer a faster and more efficient alternative for predicting the performance of the airfoil and allow non-CFD experts to obtain accurate estimation of the aerodynamic performance.

Two machine learning algorithms are considered in this study, Random Forests and Neural Networks to estimate the aerodynamic coefficients from the CFD simulation data detailed in Section 5.3. The dataset includes results for angles of attack ranging from -5 to 15 degrees, across different Reynolds numbers and surface conditions: clean, roughness and erosion. To reduce the complexity of the study only the lift coefficient has been considered.

Random Forests are an ensemble learning method that operates by constructing different decision trees during the training and performs a regression between the individual trees to perform an estimation. They are robust to overfitting, especially with large datasets, and can handle a mixture of numerical and categorical data. Moreover, Random Forests require less feature engineering and are relatively easy to implement and interpret.

On their side, Neural Networks (Castorrini, Ortolani, Minisci, & Campobasso, 2024) (Cappugi, Castorrini, Bonfiglioli, Minisci, & Campobasso, 2021)have shown remarkable success, in capturing complex relationships in data through multiple layers of nonlinear transformations. They are highly flexible and can model intricate patterns in large datasets, making them suitable for high-dimensional, nonlinear problems such as the one in question. However, they require substantial data for training and have a risk of overfitting.

Table 13 Advantages and disadvantages of the machine learning algorithms considered.

Algorithm	Advantages	Disadvantages
Random Forests, RF	Robustness to overfitting due to ensemble averaging	Can be computationally intensive for very large datasets
	Capability to handle large datasets with different types of variables (categorical, numerical ...)	May require significant memory for storing multiple trees
	Less need for extensive feature engineering	Less effective for extrapolating beyond the range of training data
	Good performance with minimal tuning	Predictions can be less smooth compared to continuous models
	Provides feature importance, aiding in model interpretability	
Neural Networks, NN	High flexibility in modelling complex and non-linear relationships	Requires large amounts of data for effective training
	Can handle very large and high-dimensional datasets effectively	May require specialized hardware and can be computationally intensive

Suitable for capturing interactions between variables	Prone to overfitting without proper regularization
Potential to achieve high accuracy with proper tuning and sufficient data	Require extensive hyperparameter tuning and are challenging to interpret

To perform the comparison the NACA 2421 airfoil has been employed. This airfoil does not belong to the dataset employed to train the models. Moreover only 16 random airfoils from the dataset were employed to train the model. This reduced dataset was composed by the first 16 airfoils that were completely simulated. The models were not intensively tuned as it one of the objectives was to analyse how well they performed without proper tuning. Hereunder, the results of both models are compared for lift coefficient prediction. Figure 42, Figure 43 and Figure 44 present the results at three different erosion conditions: soft ($h_e = 0.001$, $l_e = 0.02$ and $u_e = 0.01$), milde ($h_e = 0.004$, $l_e = 0.04$ and $u_e = 0.04$) and hard ($h_e = 0.008$, $l_e = 0.04$ and $u_e = 0.04$) respectively. Yellow stars represent the estimations while the blue dots the CFD results.

It can be seen how for the soft erosion, Figure 42, both models performed adequately showing higher discrepancies at higher angles of attack while the stall behaviour is captured by both of them. The better agreement is found at angles between 0 and 5 degrees. This is not the case for the other two conditions.

The Random Forest algorithm starts to missbehave when the erosion is increased (Figure 43) and dramatically fails to estimate under hard erosion (Figure 44). A good agreement is obtained at angles lower than 5 degrees on mild conditions but no accuracy is found on hard conditions. The Neural Networks clearly outperform the Random Forest algorithm at mild and hard conditions. Deviations from CFD results are found at high and low angles of attack but the model cualitatively agrees on these two conditions. It is thought that both models would be improved if the full dataset is employed.

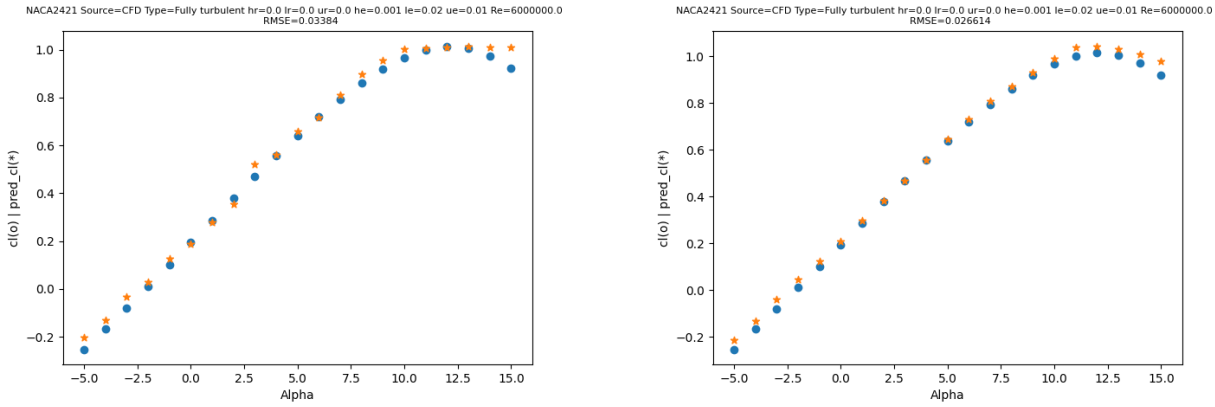

a) *Random forest* b) *Neural networks*

Figure 42 Estimation of lift coefficient of the NACA 2421 airfoil. Random Forest (a) and Neural Networks (b) results are compared. Reynolds number of 6 million, soft erosion $h_e = 0.001$, $l_e = 0.02$ and $u_e = 0.01$.

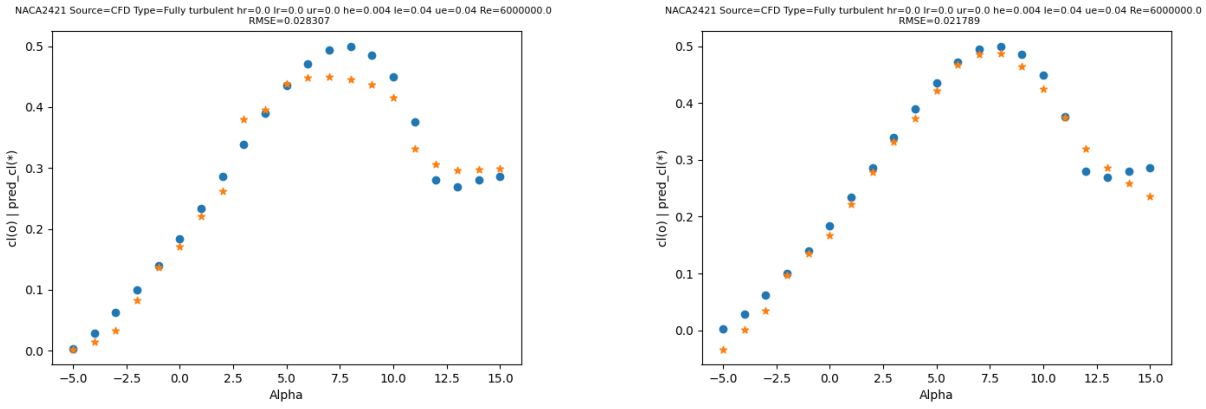

a) *Random forest* b) *Neural networks*

Figure 43 Estimation of lift coefficient of the NACA 2421 airfoil. Random Forest (a) and Neural Networks (b) results are compared. Reynolds number of 12 million, mild erosion $h_e = 0.004$, $l_e = 0.04$ and $u_e = 0.04$.

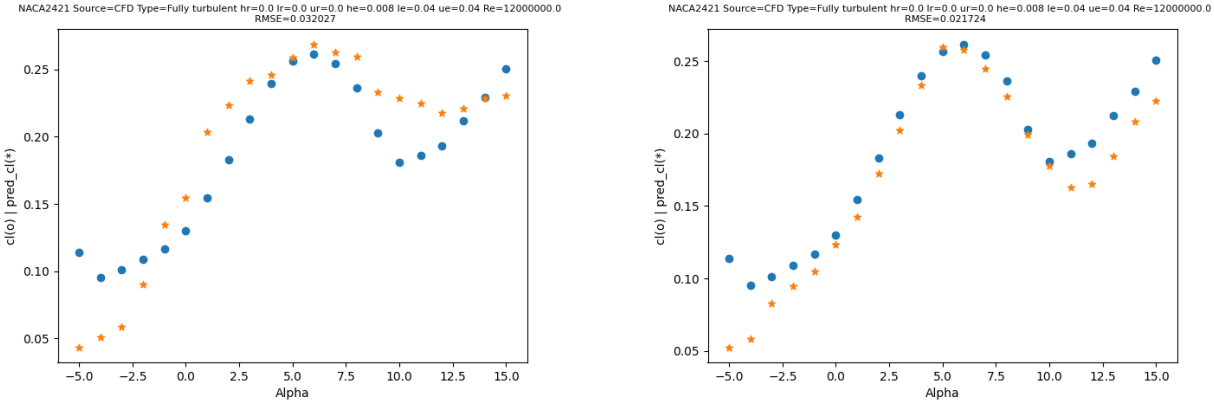

1. *Random forest* 2. *Neural networks*

Figure 44 Estimation of lift coefficient of the NACA 2421 airfoil. Random Forest (a) and Neural Networks (b) results are compared. Reynolds number of 12 million, hard erosion $h_e = 0.008$, $l_e = 0.04$ and $u_e = 0.04$.

Due to the lack of accuracy, both quantitative and qualitatively, of the Random Forest (Figure 44a) the model is discarded, and the final models are developed based on Neural Networks. Table 14 shows the root mean square errors (RMSE) of the three cases considered. It must be noted that the RMSE values are not normalized and therefore it cannot be used to compare the three conditions between them. The RMSE values show how the Neural Network algorithm always outperforms the Random Forest.

Finally, it is thought that developing a model for rough conditions and other for eroded conditions can be beneficial resulting in higher levels of accuracy.

Table 14 RMSE values of the three cases considered.

Case	Random Forest	Neural Networks
Soft erosion and Reynolds 6 million	0.034	0.026
Mild erosion and Reynolds 12 million	0.028	0.022
Hard erosion and Reynolds number	0.032	0.022

After the preceding study the following decisions were made:

- Neural Networks algorithm will be employed.

- A model will be developed to predict each condition, roughness and erosion. Both will be able to estimate clean conditions.
- Each coefficient (lift, drag and efficiency) will be estimated by a separate model.

Six models will be developed based on the aforementioned decisions.

5.5 Results and tool evaluation

Training a neural network involves adjusting its parameters (weights and biases) to minimize the difference between its predictions and the actual values. The following steps are followed:

1. Initialization: the network's weights and biases are initialized randomly.
2. Forward propagation: input data is passed through the network layer by layer. Each neuron computes a weighted sum of its inputs and applies the activation function to produce its output. This process continues until the final layer where the network gives its estimation.
3. Loss computation: the prediction is compared to the actual value using a loss function quantifying the difference between the values.
4. Backward propagation: the gradients of the loss function are computed with respect to each weight and bias. These gradients represent the contribution of each parameter to the overall loss.
5. Gradient descent optimization: the weights and biases are updated using an optimization algorithm (gradient descent) adjusting the parameters in the direction that reduces the loss and scale by the so-called learning rate.
6. Iteration: the process of forward and backward propagation is repeated for multiple iterations over the entire training dataset until the loss converges to a minimum value or other stopping criteria. This process can be manual in order to diminish the risk of overfitting.
7. Validation: the obtained model is periodically evaluated on a separate validation dataset. For the roughness models, the entire dataset has been split using an 80% of the data to train the model and a 20% to validate the model. This allows to monitor the overfitting and adjusting the hyperparameters as learning rate, batch size and architecture.
8. The parameters are tuned to improve the result and the whole workflow is followed again until the desired level of accuracy is reached.

Table 15 presents the architecture of the models (number of layers and nodes per layer) employed on the six models that have been developed within this study.

Table 15 Number of layers and nodes per layers employed in each of the six developed models

Model		Layers	Nodes per layer
Roughness	Lift	4	512
	Drag	4	512
	Efficiency	2	200 and 100
Erosion	Lift	2	500 and 250
	Drag	2	500 and 250
	Efficiency	2	500 and 250

5.5.1 Roughness model

As detailed in Section 5.1, two parametrizations of the geometry where considered: PARSEC and Bezier (xiyi). The PARSEC parametrization employs "physical" parameters, as the radius at the leading edge, while the Bezier parametrization uses the coordinates of control points. The PARSEC parametrization does not allow to retrieve complex geometries as the airfoil CA00121 while the Bezier performs accurately on the retrieval of the original airfoil shape.

The Bezier parametrization is the one that will be employed on the final model as:

- It allows to retrieve complex geometries
- It is employed in the parametrization of the CENER's airfoil design tool

the accuracy of a model trained with this parametrization will be compared against a similar one employing the PARSEC parameters.

The full dataset has been employed to train and validate the model, using the 80%-20% guideline. Only clean and rough conditions have been considered. To test the model, the DU93W210 airfoil was excluded from training and validation stages. The architecture employed on both models is the presented on Table 15.

To evaluate the models two main metrics have been employed: the root mean square error (RMSE) and the R-squared (R2).

The RMSE is a measure of the differences between the predicted values by a model and the actual values observed (CFD results). It is defined as the square root of the average of the squared differences between the predicted and actual values. Mathematically,

$$RMSE = \sqrt{\frac{1}{n}\sum_{i=1}^{n}(y_i - \hat{y}_i)^2}$$

where n is the number of observations, y_i and $\hat{y}_i$ are the actual and predicted values of the i-th observation respectively. This metric is scale-dependent and penalizes large errors. The lower it is the more accurate is the model.

The R-squared (R2) metric is a statistical measure that quantifies how well the regression model captures the variability of the data. It can be understood as how well the polar curve is captured. Its value ranges from 0 to 1. An R2 of 1 indicates that the model explains all the variability of the actual data while a value of zero indicates that the prediction does not represent the actual data. The closer to 1 is the R2 the better represented is the data. Mathematically,

$$R^2 = 1 - \left(\frac{\sum_{i=1}^{n}(y_i - \hat{y}_i)^2}{\sum_{i=1}^{n}(y_i - \bar{y})^2}\right)$$

where $\bar{y}$ represents the mean value of the observations.

All the simulated conditions of the DU93W210 have been compared. Table 16 collects the mean values of the metrics of the 84 conditions that were simulated. PARSEC parametrization obtains better accuracy on lift and efficiency coefficients while drag is better estimated with the Bezier parametrization. Nevertheless, both models result in really good agreement with the CFD results as the RMSE and R2 metrics show. As an example, Figure 45 shows the efficiency curves of the DU93W210 airfoil at Reynolds number of 9 million and $h_r = 0.0005$, $l_r = 0.1$ and $u_r = 0.2$. On the left, Figure 45 (a) the estimations obtained with PARSEC parametrization is shown while Bezier predictions are depicted in Figure 45 (b). As it can be seen in this example, both estimations are promising. Even the metrics are better for the PARSEC model, the Bezier results agree more with the CFD results at higher angles of attack and those close to the maximum efficiency. This is seen also in other cases.

Due to the benefits of the Bezier parametrization and its proven capability to obtain accurate results this is the modelling approach followed to obtain the final model.

Table 16 Comparison of the metrics between the two considered parametrizations.

Parametrization	**Coefficient**	**RMSE**	**R2**
PARSEC	Lift	0.0188	0.998

	Drag	0.0036	0.983
	Efficiency	3.767	0.969
BEZIER	Lift	0.0612	0.979
	Drag	0.0023	0.994
	Efficiency	5.177	0.939

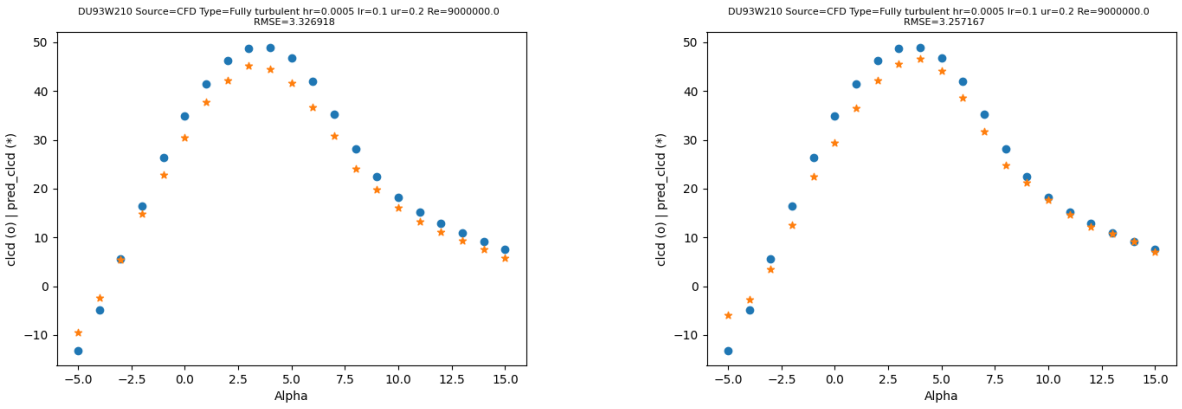

a) *Random forest* b) *Neural networks*

Figure 45 Efficiency curves obtained with PARSEC (a) and Bezier (b) parametrizations. Conditions are $Re = 9$ million, $h_r = 0.0005$, $l_r = 0.1$ and $u_r = 0.2$.

After this comparison and the decision of employing the Bezier parametrization, the hyperparameters of the roughness model have been tuned to improve its accuracy. New tests have been performed to assess the accuracy of the new model.

The first test is intended to demonstrate the capability of the model to accurately estimate the aerodynamic performance under different roughness conditions. Airfoils that have been considered on the training dataset are now tested on different conditions of those included in the training dataset. Table 17 shows the parameters employed in this test.

Table 17 Parameters to test the estimation capabilities of new conditions for known airfoils.

Airfoil	*Re* (millions)	u_r	l_r	h_r	Total curves
DU95W180	7.5, 8, 10	0.1	0.1	0, 2e-4, 3.5e-4	9
DU97W300	7.5, 8, 10	0.1	0.1	0, 2.5e-4, 3.5e-4	9
NACA63-418	7, 9, 11	0.13, 0.18	0.13, 0.18	0, 2e-4, 3.5e-4	27

For each airfoil in Table 17, the R-squared metric has been employed to analyse the accuracy of the estimations. Figure 46 shows the mean values of the R-squared metric which are all above 0.98. The results demonstrate the capability of the model to perform accurate estimations of known airfoils under new roughness conditions and Reynolds numbers. Figure 47, presents the minimum value of the metric per each airfoil. Worst results are obtained for the NACA63-418 airfoil on clean conditions and Reynolds number of 11 million with a value of the R-squared metric of 0.93 for the lift coefficient.

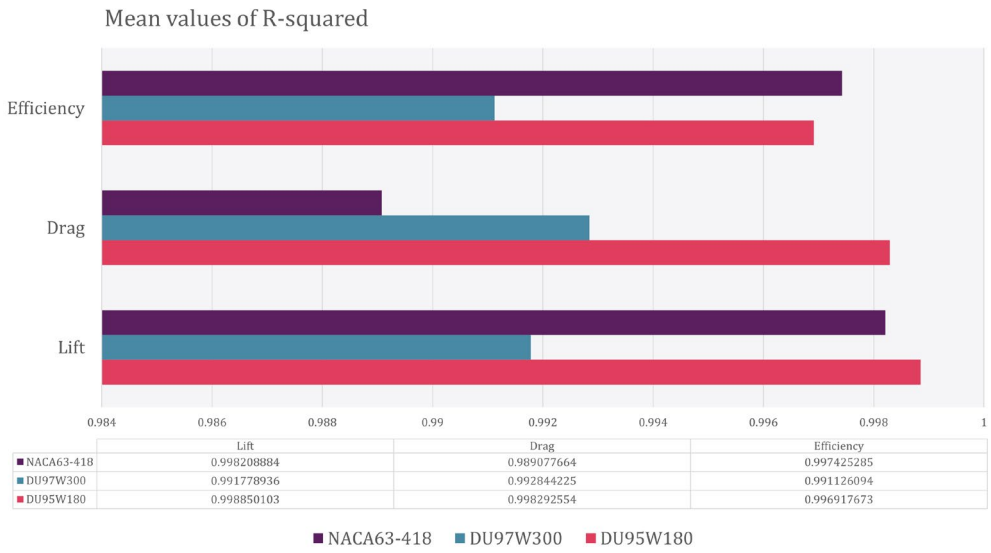

	Lift	Drag	Efficiency
NACA63-418	0.998208884	0.989077664	0.997425285
DU97W300	0.991778936	0.992844225	0.991126094
DU95W180	0.998850103	0.998292554	0.996917673

Figure 46 Mean values of the R-squared metric for each airfoil considered in Table 17.

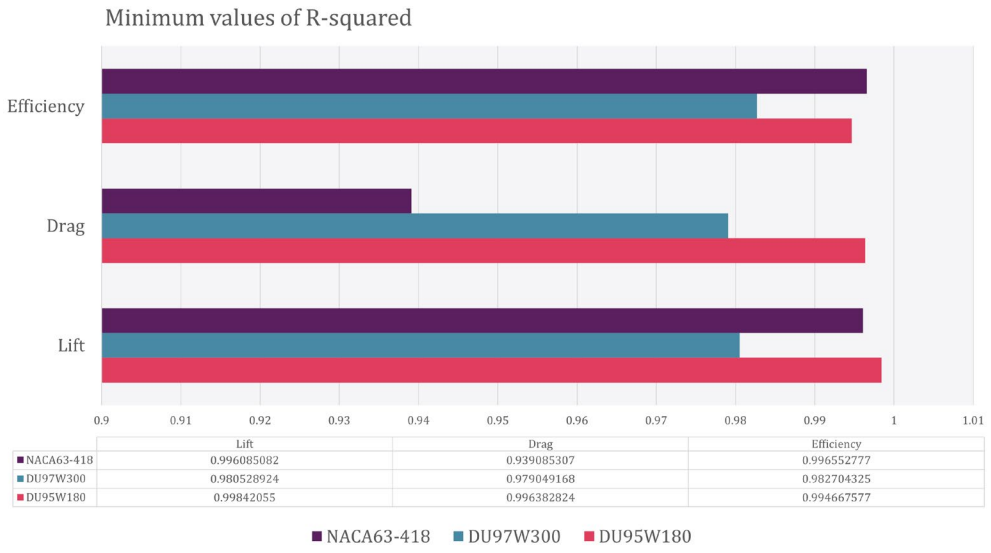

	Lift	Drag	Efficiency
NACA63-418	0.996085082	0.939085307	0.996552777
DU97W300	0.980528924	0.979049168	0.982704325
DU95W180	0.99842055	0.996382824	0.994667577

Figure 47 Minimum values of the R-squared metric for each airfoil considered in Table 17.

For the worst estimation, the lift and drag curves are shown in Figure 48. It is believed that, even in the worst case, the estimations correlate adequately with the CFD results and that the level of accuracy, RMSE of 0.0375 and 0.00164 for lift and drag curves respectively, is more than satisfactory. It must be noted that the greater deviations from CFD results occur at higher angles of attack where there are less data on the dataset.

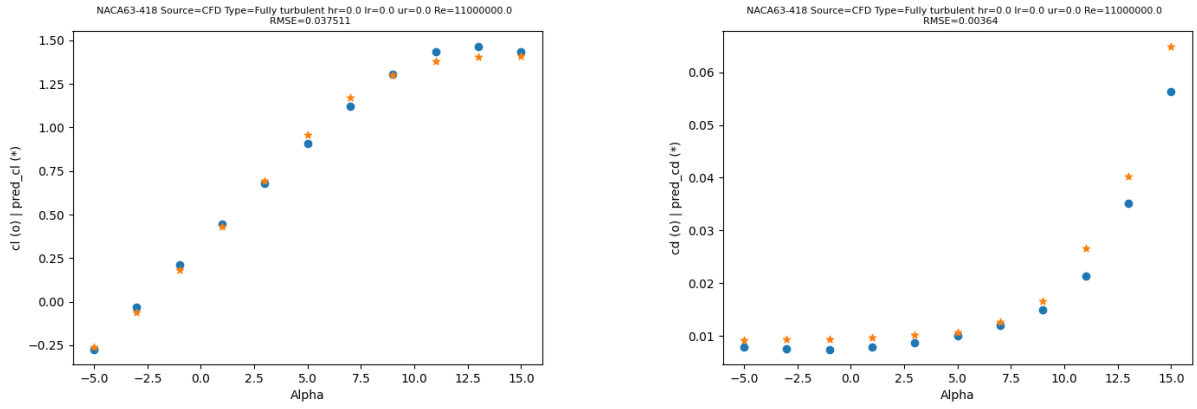

a) *Lift coefficient* b) *Drag coefficient*

Figure 48 Lift (a) and Drag (b) curves of the worst estimation, corresponding to the NACA 63-418 airfoil on clean conditions and Reynolds 11 million.

Another test has been performed in order to assess the range of applicability of the model. Six new airfoils have been simulated and the CFD results are compared to the estimations of the model. Table 18 collects the conditions simulated to test the ability of extrapolation of the model. Three airfoils are expected to be wrongly estimated: FFAW3360, as it has a thickness of 36% which is over the maximum thickness considered and the two CA airfoils, they present complex thickness and camber curves and only one airfoil on the dataset present those characteristics. Moreover, it is also expected lower accuracy on the predictions.

Table 18 Test cases with new airfoils and conditions considered within the dataset.

Airfoil	*Re* (millions)	u_r	l_r	h_r	Total curves
FFAW3211	6	0.1, 0.2	0.2	0, 2.5e-4	3
L5T14Tunel	9	0.2	0.1, 0.15	0, 5e-4	3
S820	6, 12	0.15	0.15	0, 2.5e-4	4
ca00318bte300	9	0.2	0.2	0, 1e-4, 2.5e-4, 5e-4	4
ca00224bte300	9	0.1	0.1	0, 1e-4, 2.5e-4, 5e-4	4
FFAW3360	6	0.1, 0.2	0.1, 0.2	0, 2.5e-4	5

Figure 49 shows the mean values of the R-squared metric for the six airfoils that have not been considered in the dataset. As expected, FFAW360 and ca00224bte300 are erroneously estimated. This was expected as these airfoils are out of the range of shapes considered in the dataset. As the ca00318bte300 has a lower thickness than ca00224bte300 (18% and 24% respectively), its estimation is more accurate. Surprisingly, this airfoil presents good agreement with CFD results for the lift coefficient while drag and efficiency are worse predicted. Really promising estimations are obtained for the L5T14tunel and S820 with values of R-squared metric higher than 0.95 for lift, drag and efficiency coefficients. Nevertheless, poor estimations were obtained for the FFAW3211 airfoil that were unexpected.

	Lift	Drag	Efficiency
ca00318bte300	0.94449712	0.776123217	0.766160523
ca00224bte300	0.886919666	0	0
S820	0.994294528	0.948996333	0.975770311
L5T14tunel	0.989712891	0.977125208	0.96395155
FFAW3360	0	0	0
FFAW3211	0.63625896	0.624075622	0.709308772

Figure 49 Mean values of the R-squared metric for airfoils not considered in the dataset.

In order to understand why this airfoil is poorly estimated, the geometry parameters of the six new airfoils are compared to the statisctical distribution of the parameters considered in the dataset. This comparison is presented in Figure 50. Both of the FFA airfoils as well as the ca00224bte300 have parameters outside of the whiskers. The whiskers represent 1.5 times the interquartile range. The ca00318bte300 airfoil also present some, but fewer than the other 3 miss estimated airfoils, parameters outside of the whiskers. This results in poorer estimation of the drag and efficiency coefficients. This is not the case of the L5T14tunel and S820 airfoil which are contained within the whiskers limits and their estimations totally agree with the CFD results.

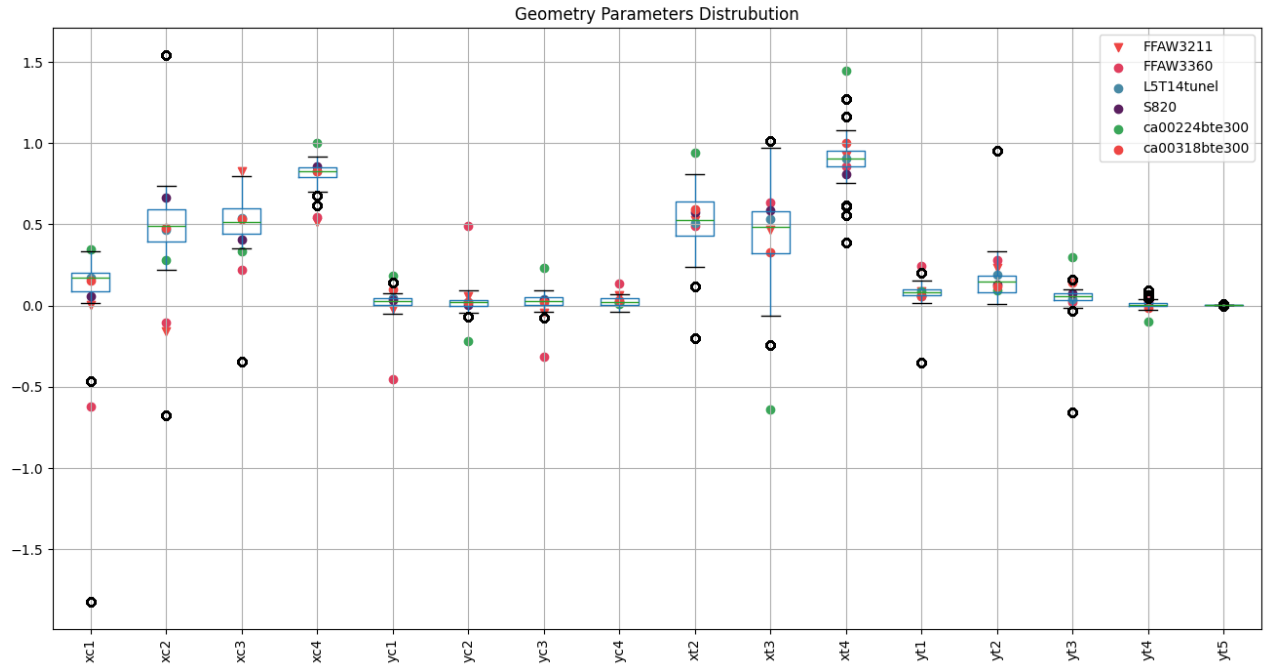

Figure 50 Comparison of the geometry parameters of the new airfoils compared to the values of the parameters considered within the dataset.

For instance, Figure 51 shows the lift and drag coefficients estimated for the L5T14tunel airfoil. Really good agreement between estimations (yellow stars) and CFD results (blue dots) is found considering that the airfoil is not considered within the dataset and that the aerodynamic behaviour is highly related to the airfoil's shape.

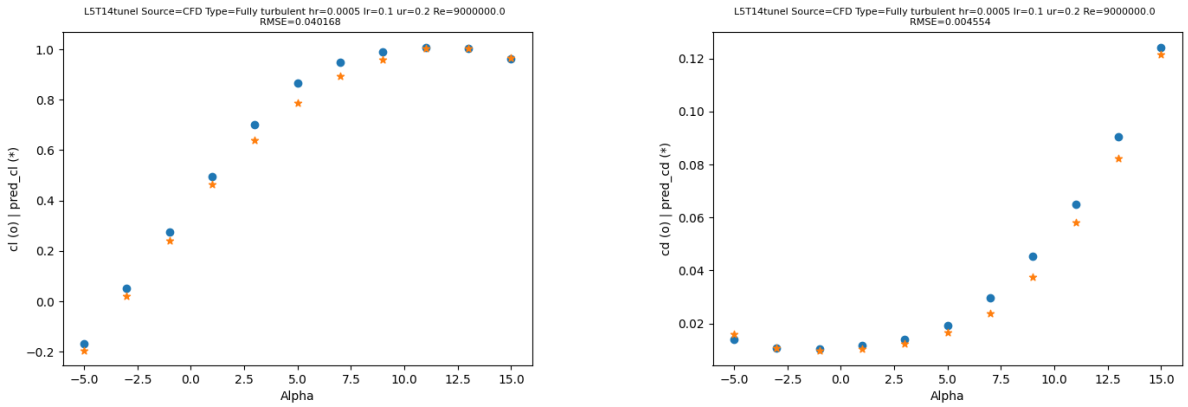

a) *Lift coefficient* b) *Drag coefficient*

Figure 51 Estimations of the lift and drag coefficient of the L5T14tunel airfoil. The results correspond to the following simulated condition: $Re = 9$ million, $h_r = 0.0005$, $l_r = 0.1$ and $u_r = 0.2$.

It is concluded that:

- The roughness model has accurate performance on the estimation of roughness conditions for the airfoils considered within the dataset.
- The roughness model is able to extrapolate the estimations to new airfoils whose parameters are contained within the whiskers of the geometry parameters statistical distribution.
- The roughness model cannot be employed to estimate the aerodynamic behavior of airfoils whose parameters are outside of the range of application. This range of application is defined by the whiskers of the geometry parameters.
- The roughness model is a highly valuable tool that can be further developed and improved to obtain even more accurate predictions.

5.5.2 Erosion model

As already explained the airfoil performance model is composed by 6 individual models one per surface condition and one per aerodynamic coefficient. After developing the final erosion model and all the knowledge gathered by CENER's team, the erosion ML model is developed. Once the simulations are completed and the dataset is populated, a different validation strategy was followed. To reduce the resources needed for the development, one random condition per airfoil was excluded from the training and validation stages. In addition, the convergence rate of the eroded condition is lower than that of the rough simulations resulting in less data available. These conditions are employed to test the model and determine how it performs. With the remaining data the 80%-20% split was followed to create the training and validation tests. Table 19 presents the conditions that have been randomly selected to test the erosion model.

Table 19 Conditions excluded from training and validation phases. These conditions are employed to assess the accuracy of the erosion model.

Name	he	le	ue	Re
AG25	0.001	0.04	0.02	6000000
AH79-100	0.004	0.01	0.04	9000000
B29	0.008	0.02	0.02	12000000

CLARK-YM18	0.001	0.02	0.01	6000000
DEFIANT-BL20	0.004	0.01	0.02	12000000
DFVLR-R4	0.001	0.02	0.01	6000000
DU91W2250	0.004	0.01	0.04	12000000
DU93W210	0.008	0.01	0.01	6000000
DU95W180	0.001	0.04	0.01	9000000
DU96W180	0.004	0.04	0.01	9000000
DU97W300	0.008	0.01	0.02	12000000
EPPLER1098	0.001	0.04	0.02	6000000
HUGHES-HH-02	0.004	0.02	0.02	9000000
L4T17tunel	0.008	0.02	0.04	12000000
L6T9tunel	0.001	0.02	0.01	6000000
MH93-16	0.001	0.01	0.02	9000000
MS1-0313	0.008	0.02	0.04	6000000
NACA63-418	0.004	0.02	0.02	9000000
NACA63-421	0.001	0.04	0.04	12000000
NACA64-618	0.008	0.04	0.04	6000000
RONC1046	0.001	0.01	0.01	6000000
S809	0.008	0.02	0.02	6000000
S814	0.008	0.02	0.01	12000000
S827	0.001	0.04	0.01	9000000
WB-135-35	0.004	0.02	0.04	6000000
ca00121bte300	0.008	0.01	0.01	9000000

From the estimations performed by the erosion model, the R-squared metric has been computed. The mean values over the 26 conditions tested are presented in Table 20. As can be seen, the estimations correlate adequately with the CFD results employed to train the model.

Table 20 Means values of the R-squared metric obtained on the test of the erosion model.

Coefficient	Lift	Drag	Efficiency
Mean value of R2 metric	0.99	0.95	0.98

The individual values of the R-squared metric of each test conducted are presented in Figure 52. The erosion model is able to estimate adequately the influence of the erosion on the aerodynamic performance. The minimum value of the lift coefficient is 0.95 and is obtained for the DU97W300 airfoil which is one of the thickest airfoils analysed. The drag coefficient is the worst estimated with a mean value of 0.94. Among all the tests, the drag coefficient is poorly estimated on the MS1-0313 airfoil. Nevertheless, as the efficiency is estimated with a separate model the minimum R-squared value of the efficiency is 0.94.

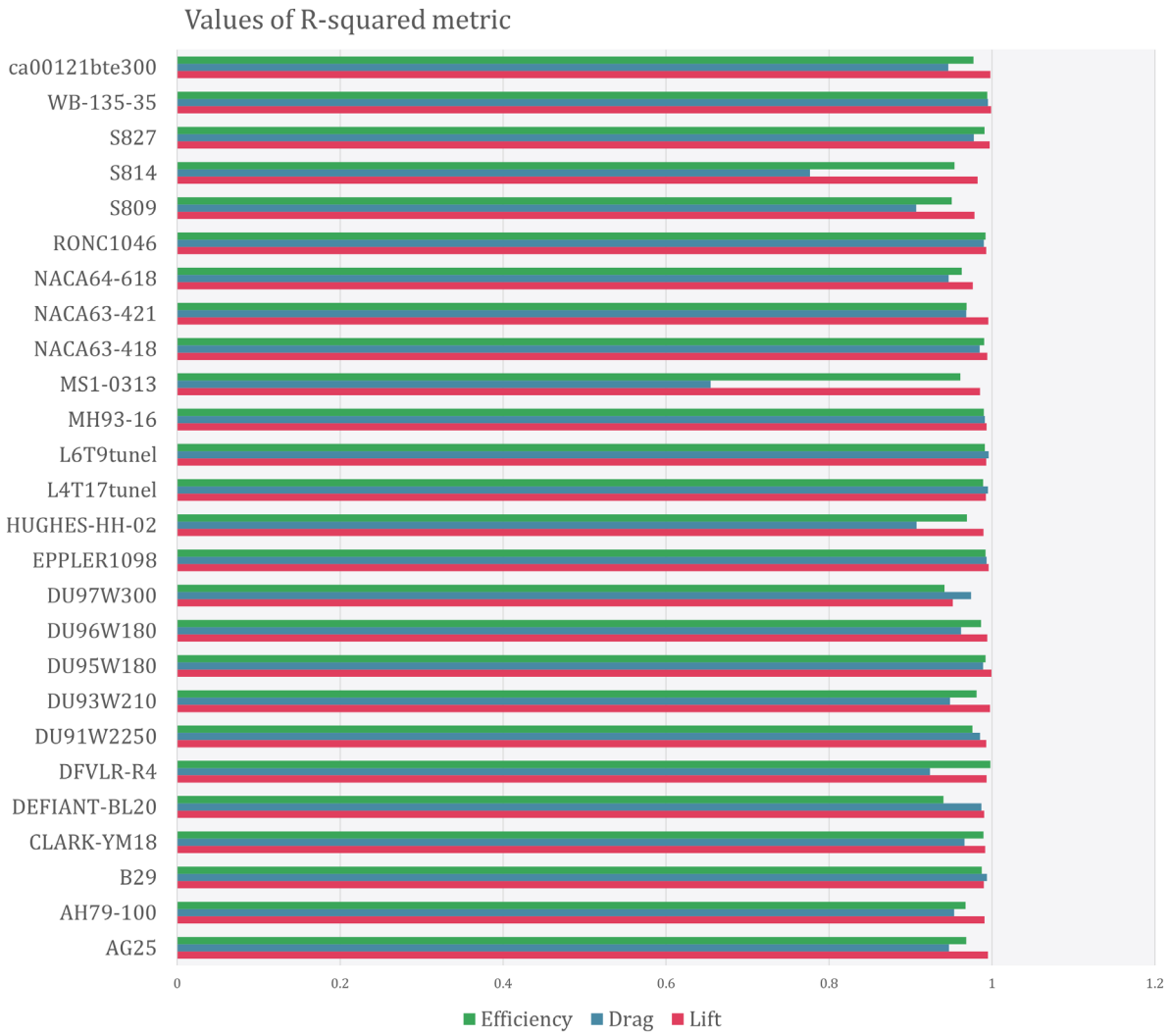

Figure 52 Values of the R-squared metric obtained on the 26 tests performed.

Figure 53 shows the worst results obtained by the erosion model. Even though the corresponding R-squared metric is 0.65, the root mean square error is 0.0035 presenting higher deviation from CFD results at angles higher than 5 degrees.

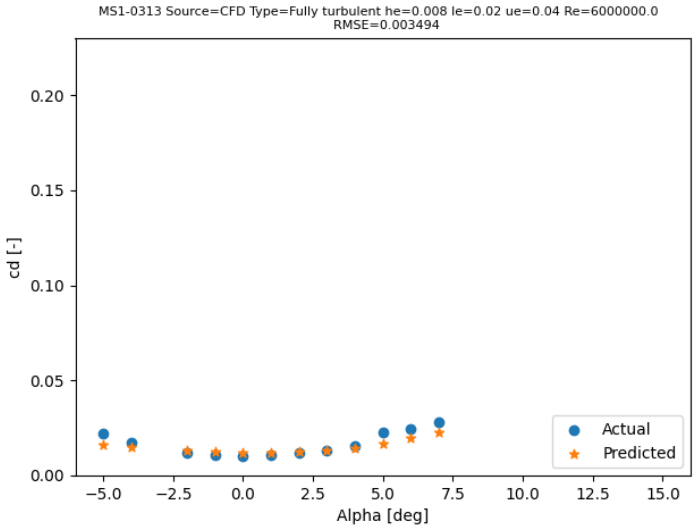

Figure 53 Drag prediction of the MS1-0313 airfoil under hard erosion conditions ($h_e = 0.008$, $l_e = 0.02$, $u_e = 0.04$) and Reynolds number of 6 million.

Figure 54 presents the predicted lift and drag curves of the DU9142250. The curves present an R-squared metric of 0.993 and 0.985 respectively with RMSE of 0.034 and 0.0044. Lift coefficients present more deviations at angles from 0 to 3 degrees while the drag deviates the more at angles of attack higher than 7 degrees.

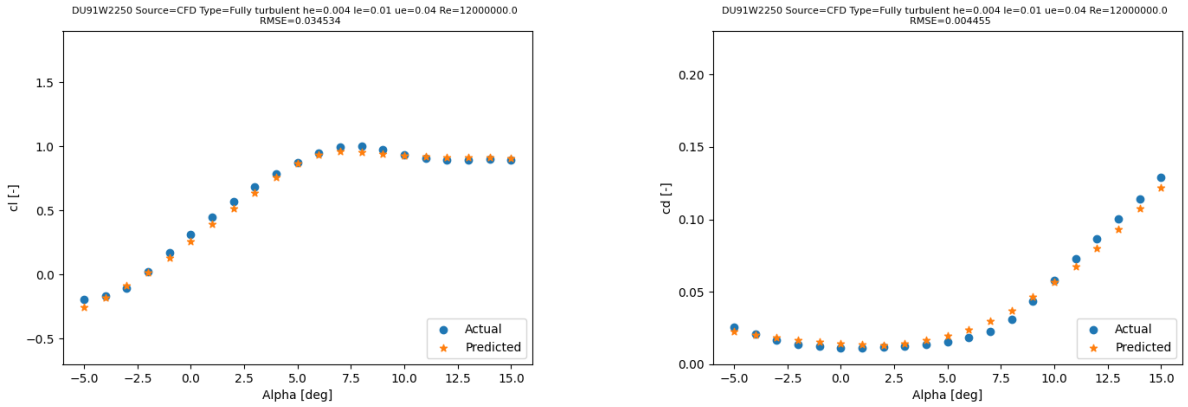

a) Lift coefficient *b) Drag coefficient*

Figure 54 Lift (a) and drag (b) prediction of the DU91W2250 airfoil under mild erosion conditions ($h_e = 0.004$, $l_e = 0.01$, $u_e = 0.04$) and Reynolds number of 12 million.

Further assessment of the accuracy and range of applicability of the erosion model will be undertaken. Even though, it is believed that these results are promising. The modelling of the erosion with a CFD approach requires of time and experienced people to be carried. The present erosion model allows a non-CFD expert to obtained reasonably accurate results for all of the airfoils considered within the dataset.

6 Conclusions

An extensive study on the erosion and roughness influence over airfoil performance has been done. The main output of this study is an Airfoil Performance Model for eroded and rough conditions that will be used in future tasks to obtain the AEP of wind turbines and wind farms operating under special weather conditions. From the present work it has been concluded that:

- For rough conditions, two turbulence models have been compared: fully turbulent and transitional. The employment of a transitional turbulence modelling does not imply a substantial improvement of the fully turbulent approach. The fully turbulent approach is employed on the dataset generation.
- The tool Construct2D eases the grid generation on airfoils in clean and rough conditions. Its employment allows an optimal automation of the simulation workflow.
- Equivalent sand grain heights are obtained with the Cebeci & Bradshaw model. Different values are employed in the dataset generation. The values are aligned with the damage categories of the SALT tool and IEA Task 46.
- From the studies in OREC experimental wind turbine, it is concluded that small AEP losses due to blade erosion cannot be accurately monitored using SCADA-based power curve analysis, given the uncertainty in power measurements. The discrepancies between the SALT tool and SCADA-derived power curves can be attributed to the idealised conditions assumed by the SALT tool, which generally align with the outermost data points of the true data.
- From the studies in OREC experimental wind turbine, it is concluded that despite the limitations of SCADA data in erosion monitoring, the SALT tool remains valuable for operational and maintenance (O&M) teams. If inspection images can be labelled for erosion defects and automatically integrated into the SALT tool, it can provide estimations of AEP losses due to LER. Tracking changes in these values over multiple inspections can guide decision-making based on tangible monetary losses rather than only drone inspection images. It is vitally important that the categorisation of LER remains constant throughout this process.
- A drone inspection performed in Alaiz will be the basis to study the dynamic evolution of erosion and dirtiness for in-service blades
- To ensure high quality meshes with leading edge erosion, the erosion shape has been modified. A slope of 45 degrees has been employed at the transition between affected and non-affected areas. The tool Construct2D is used to generate these grids.
- The influence of the erosion on the DU95W180 airfoil is analysed. Erosion heights corresponding to different erosion categories are considered. It has been observed that the erosion can produce a decrease on the maximum efficiency up to 34.4% and reduce the angle of attack where maximum efficiency takes place.
- The influence of Reynolds number is assessed on the most damaging erosion cases. The deterioration of the aerodynamic performance increases with Reynolds number. Nevertheless, aerodynamic curves do not present significant differences. In fact, the difference between maximum efficiencies at different Reynolds (on eroded cases) is less than 4%.
- The Reynolds numbers analysed correspond to those of the 50% outermost part of modern wind turbine blades. They will be employed on the dataset generation.
- 39 airfoils are considered on the dataset. Their thickness ranges from 10 to 30 %.
- Two geometry parametrizations have been compared: PARSEC and Bezier. The Bezier parametrization is employed. It allows to characterize complex airfoil shapes as well as to retrieve the original geometry from them.

- A dataset composed by more than 100,000 angles of attack is employed to develop the Airfoil Performance Model.
- Two ML algorithms have been compared: Random Forest and Neural Networks. It has been proven that NN are more accurate than RF and APM will be based on them.
- APM is composed by 6 model one by status (roughness and erosion) and one per coefficient (llift, drag and efficiency).
- The influence of the geometry parametrization has been analyzed. The PARSEC parametrization result in more precise estimations. Even though, the Bezier parametrization yields to accurate enough predictions. Due to the advantageous characteristics of the Bezier parameters, it is employed on the APM development.
- The ML model have been developed and optimized to accurately predict the influence of roughness and erosion on the aerodynamic behavior of the airfoil.
- APM is able to yield accurate predictions under new roughness conditions for the airfoils considered within the dataset.
- It has been observed that APM is not able to properly predict new airfoil outside of the range of application. If the geometric parameters of the airfoil are outside this applicability range, the estimations cannot be considered adequate.
- The prediction under erosion of the aerodynamic performance is accurate for the airfoils that compose the dataset. The employment of one model per coefficient ensures that the accuracy of each coefficient prediction is independent. In the worst analyzed case, the RMSE is low enough and demonstrates the versatility of the APM.

7 Deviations

Two technical issues have been detected for Task 3.3, they are explained in this deliverable for the shake of traceability.

PLOCAN had an issue with the boat that get service to their wind turbine. The boat is ready for operation. PLOCAN is currently doing all the arrangements necessary to perform the experimental campaign. The best time window is the second or third week of September. This experimental campaign will yield very interesting results to create new entries to the **database** developed in Task 3.3.

In addition, a deviation occurred with regard **DTU´s contribution to Task 3.3**: DTU needs the results of the experiments done in another project, LERCat, to complete their work in Task 3.3. The LERCat project suffered technical issues in the wind tunnel and good quality results are not available yet.

Both PLOCAN experimental campaign and DTU contribution will be included in the second version of this deliverable.

These facts will not have an impact on other tasks and deliverables. Task 4.4 is the only activity that uses the outputs from Task 3.3. Since the Airfoil performance model is ready no impact or delays are foreseen.

8 References

Cappugi, L., Castorrini, A., Bonfiglioli, A., Minisci, E., & Campobasso, S. M. (2021). Machine learning-enabled prediction of wind turbine energy yield losses due to general blade leading edge erosion. *Energy Conversion and Management, 245*, 114567. doi:https://doi.org/10.1016/j.enconman.2021.114567

Castorrini, A., Ortolani, A., Minisci, E., & Campobasso, M. S. (2024). Opensource machine learning metamodels for assessing blade performance impairment due to general leading edge degradation. *Journal of Physics: Conference Series*, 052055. doi:10.1088/1742-6596/2767/5/052055

Cebeci, T., & Bradshaw, P. (1997). *Momentum Transfer in Boundary Layers.* Hemisphere Publishing Corporation.

Cousteix, J. (1989). *Turbulence et couche limite.* Cèpaduès-éditions.

Jonkman, J., Butterfield, S., Musial, W., & Scott, G. (209). *Definition of a 5-MW Reference Wind Turbine for Offshore System Development.* National Renewable Energy Lab. (NREL), Golden, CO (United States), United States. doi:10.2172/947422

Maniaci, D., & White, E. (2022). *Owner Reports - Airfoil Performance Degradation due to Roughness and Leading-edge Erosion.* United States. doi:https://doi.org/10.21947/1373097

Saenz, E., Méndez-López, B., & Muñoz, A. (2022). Effect of erosion morphology on wind turbine production losses. *Journal of Physics: Conference Series, 2265*, 032059. doi:10.1088/1742-6596/2265/3/032059